Ecological Modelling 478 (2023) 110210

Contents lists available at ScienceDirect

Ecological Modelling

journal homepage: www.elsevier.com/locate/ecolmodel

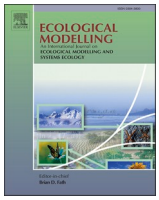

Modelling fine scale route choice of upstream migrating fish as they approach an instream structure

J.R. Kerr [a,*], J.S. Tummers [b,1], T. Benson [c], M.C. Lucas [b], P.S. Kemp [a]

[a] International Centre for Ecohydraulics Research, Faculty of Engineering and Physical Sciences, University of Southampton, Boldrewood Campus, Southampton SO16 7QF, UK
[b] Department of Biosciences, University of Durham, South Road, Durham DH1 3LE, UK
[c] HR Wallingford, Howbery Park, Wallingford OX10 8BA, UK

ARTICLE INFO

Keywords:
Lamprey
Hydropower
Telemetry
Fish passage
Individual based model
Space use

ABSTRACT

This study used pattern-oriented modelling (POM) to investigate the space use and behavioural response of upstream migrating European river lamprey (*Lampetra fluviatilis*) to the two-dimensional hydrodynamic conditions created by an instream structure (triangular profile gauging weir). Passive Integrated Transponder (PIT) and acoustic telemetry were used to map the spatial-temporal distribution patterns of lamprey as they migrated upstream. Acoustic Doppler velocimetry and computer modelling were used to quantify the hydrodynamic environment. In adherence with the POM methodology, multiple movement models, incorporating increasingly complex environmental feedback mechanisms and behavioural rules were created and systematically assessed to identify which factors might reproduce the observed patterns. The best model was a spatially explicit Eulerian-Lagrangian Individual Based Model (IBM) that included two simple behaviours: 1) tortuous non-directed swimming when in low flow velocity (< 0.1 m s^{-1}) and 2) persistent directed (against the flow) swimming in moderate to high flow velocity (≥ 0.1 m s^{-1}). The POM indicated that flow heterogeneity was an important influence of lamprey space use and that simple behavioural rules (i.e. two separate movement behaviours in response to flow velocity) were sufficient to reproduce the main movement pattern observed: avoidance of flow recirculating regions near the banks. The combination of field telemetry, hydrodynamic modelling and POM provided a useful framework for systematically identifying the key factors (hydrodynamic and behavioural) that governed the space use of the target species and would likely work well for investigating similar relationships in other aquatic species.

1. Introduction

Habitat fragmentation is one of the greatest threats to global biodiversity (Liermann et al., 2012; Wilson et al., 2016; Sánchez-Bayo and Wyckuys, 2019), preventing migratory organisms from completing their life-cycles (Lucas et al., 2009) and restricting dispersal and gene flow between populations (Fluker et al., 2014; Wilkes et al., 2018). Anthropogenic riverine barriers, such as dams and weirs, are globally widespread (Grill et al., 2019), and in developed regions occur at high densities (e.g. 19.44 barriers km^{-1} in the Netherlands, Belletti et al., 2020), reflecting a long history of river engineering. The resultant fragmentation of habitat has contributed to a 76% global decline in abundance of migratory fish over the past 50 years (Deinet et al., 2020). In extreme cases, and particularly for diadromous fish that migrate between marine and freshwater environments, the fragmentation of river habitat, in combination with other stressors, can cause local extirpation (Gustafson et al., 2007; Katz et al., 2013) and ultimately extinction (e.g. Chinese paddlefish, *Psephurus gladius*: Zhang et al., 2020).

Mitigating the negative impacts of habitat fragmentation on fish caused by river infrastructure has occurred for centuries (e.g. since the 7th century in the Iberian peninsula, Kemp, 2016a), and includes the use of fish passes (Pereira et al., 2017; Kerr et al., 2021), trap and transport schemes (Boubeé et al., 2008), and modification of operational procedures (Muir et al., 2001). However, the efficacy of such approaches is often poor when considering the target species for which they were designed (e.g. fish passes: Brown et al., 2013; trap and transfer schemes:

* Corresponding author.
E-mail address: j.kerr@soton.ac.uk (J.R. Kerr).
[1] Author's present address: Reptile Amphibian Fish Conservation Netherlands (RAVON), Nijmegen, 6525 ED, Netherlands.

https://doi.org/10.1016/j.ecolmodel.2022.110210
Received 6 April 2022; Received in revised form 14 October 2022; Accepted 4 November 2022
Available online 23 January 2023

Lusardi and Moyle, 2017), and even more so when viewed from a fish community perspective (e.g. fish passes: Noonan et al., 2012; Tummers et al., 2016a; Klopries et al., 2018). One of the key reasons for low fish passage effectiveness is the lack of consideration of fish behaviour (Williams et al., 2012). Even for well-studied species, fundamental understanding of how movement behaviour is influenced by their environment is lacking, limiting transferability of the technology developed (Kemp, 2016b).

Although the need to accommodate fish response to hydrodynamics in the development of effective mitigation technologies is recognised (Kemp, 2012), understanding the mechanisms that explain the influence of the environment on behaviour can be challenging for two reasons. First, animal movement is complex, and is influenced by a combination of multiple factors acting simultaneously, such as motivational status (Kemp, 2016b; Goerig and Castro-Santos, 2017), habituation (Raderschall et al., 2011; Finger et al., 2016) and prior experience (Riotte-lambert and Matthiopoulos, 2020). Animals also switch between multiple movement modes in accordance with their broad-scale ecological needs (e.g. feeding or reproducing) or fine-scale environmental covariates (e.g. habitat type or predator density) (Gurarie et al., 2009). Second, movement data tend to be temporally autocorrelated, which makes identifying the importance of predictor variables (e.g. flow velocity, flow direction, depth, and channel geometry) difficult with standard statistical hypothesis testing (Dray et al., 2010). Autocorrelation is often an intrinsic property of biological data and, although there are ways to eliminate its effects by restricting data prior to analysis, this can reduce the relevance of ecological studies (Dray et al., 2010). Designing effective environmental impact mitigation measures requires improved knowledge of how fish respond to hydrodynamics in addition to the advancement of appropriate tools to evaluate this complex relationship (Kemp, 2012).

Individual Based Models (IBMs) provide a useful tool for investigating fish response to complex flow fields. Movement is typically modelled as iterative steps to account for temporal autocorrelation. Furthermore, the environment can be included in a spatially explicit way to investigate relationships between organism behaviour and space use (DeAngelis and Yurek, 2017). Spatially explicit IBMs are increasingly used to study fluvial ecology (e.g. Gao et al., 2016; Snyder et al., 2019; Padgett et al., 2020; Morrice et al., 2020), likely because advances in computer technology have permitted the generation and implementation of high-resolution hydrodynamic data at scales that are biologically relevant for decision making in aquatic organisms. In addition, IBMs allow for population level effects of individual movement behaviours to be systematically investigated, i.e. they allow for multiscale pattern-oriented modelling (POM) (Grimm and Railsback, 2012). The POM approach provides a framework for assessing different model structures (e.g. movement behaviours within an IBM) to identify the most relevant factors that describe the observed 'patterns', defined as any non-random behaviour of the modelled system. The goal is to identify a 'structurally realistic' model that captures, in a simple yet useful way, the system's generative mechanisms (Grimm and Railsback, 2012). Benson et al. (2021) undertook POM using spatially explicit IBMs to predict the upstream movement of juvenile European eel (*Anguilla anguilla*) in a tidal estuary. In their study, multiple scenarios were modelled with different elements of a complex behaviour, selective tidal stream transport, turned on or off within each IBM to predict the relative importance of each in facilitating up-estuary migration. Such models are useful tools for investigating the behaviours that underpin animal movement patterns and, once validated, enable users to predict the likely impacts of anthropogenic infrastructure (e.g. dams, weirs and fish passes), enhancing the conservation of vulnerable species.

Diadromous anguilliform fish, such as lamprey (e.g. *Lampetra* spp. and *Petromyzon marinus*) and eel (*Anguilla* spp.), are particularly impacted by anthropogenic infrastructure. For upstream migrating adult lamprey and juvenile eel, which do not jump and have relatively low burst swimming capability (e.g. lamprey: L. *fluviatilis*: Russon and Kemp, 2011; eel: *A. anguilla*: Vezza et al., 2020; *A. australis* and *A. reinhardtii*: Langdon and Collins, 2000), the high flow velocities encountered at even small (< 1.5 m) barriers can impede passage (Kerr et al., 2015; Tummers et al., 2018). Although lamprey and eel are heavily protected in Europe by a range of legislation (e.g. European Habitats Directive [92/43/EEC] and Bern convention [COE, 1979]), the effectiveness of mitigation measures designed to help them negotiate river infrastructure is variable (e.g. Kerr et al., 2015), and there is a bias towards conservation efforts for eel (e.g. Whitfield and Kolenosky, 1978; Jellyman and Ryan, 1983; White and Knights, 1997). There remains little understanding on the movement behaviour at instream barriers of many lamprey species, such as the European river lamprey (*L. fluviatilis*), for which upstream passage mitigation technologies tend to perform poorly (Kerr et al., 2015; Vowles et al., 2017; 2018; Tummers et al., 2016b; 2018; Lothian et al., 2020).

To aid in the conservation of vulnerable diadromous fish species, there is a need to better understand how behaviour and flow influence their movement patterns around anthropogenic river structures. To address this, this study used POM to investigate the hydrodynamic factors and behaviours that govern the space use of an at risk species, the European river lamprey, as they approached a triangular profile gauging weir. Specifically, we quantified: 1) the movement patterns of lamprey as they approached the gauging weir using acoustic and Passive Integrated Transponder (PIT) telemetry, and 2) the hydrodynamic environment encountered using acoustic Doppler velocimetry and computer modelling. By integrating the biological and hydrodynamic data obtained we were able to: 3) develop several spatially explicit IBMs that could be used to systematically assess which hydrodynamic factors and swimming behaviours were required to reproduce the movement patterns of river lamprey observed in the field. This study is both the first to track the fine-scale spatial-temporal (< 1 m, 1 Hz, respectively) movement patterns of river lamprey during their upstream spawning migration and to use IBMs to systematically assess what hydrodynamic and behavioural factors are influencing their space use. The results present a significant step forward in our knowledge on the movement ecology of this species and the methods used represent a useful framework for investigating similar relationships in other aquatic animals.

2. Methodology

2.1. Study site

The study site (latitude: 54.018884°, longitude: −0.88532951°, WGS84) was located on the River Derwent, a tributary of the Yorkshire Ouse, Northeast England, and encompassed a triangular profile gauging weir (Crump design) (20 m wide), micro-hydroelectric power station, and the downstream river reach (0.52 river kilometres [rkm], longitudinal distance along the river centreline) (Fig. 1). The Crump weir (a common type of gauging weir in the UK, Ireland and more widely in Europe) has a standard triangular profile (1:2 upstream and 1:5 downstream slopes) and at a flow-exceedance value of Q95 has a head loss of 1.31 m and a discharge of 2.78 $m^3 s^{-1}$. A 15% gradient Super Active Baffle technical fish pass (length: 11.2 m; internal width: 2.75 m) is located on the true right side of the weir (Fig. 1). The hydropower station is located on the right bank and consists of two horizontally installed Kaplan turbines (nominal power output 50 kW per turbine) (Fig. 1). During the study period (8 November to 20 December 2017), discharge at the site ranged from 10.4 to 52.3 $m^3 s^{-1}$ (mean: 26.6 $m^3 s^{-1}$).

2.2. Movement patterns

2.2.1. Field telemetry

To track the two-dimensional movement of lamprey, eight acoustic hydrophones (HTI 590 series 307 kHz) were installed between 0.035 and 0.085 rkm downstream of the weir (Fig. 1). Positioning of the

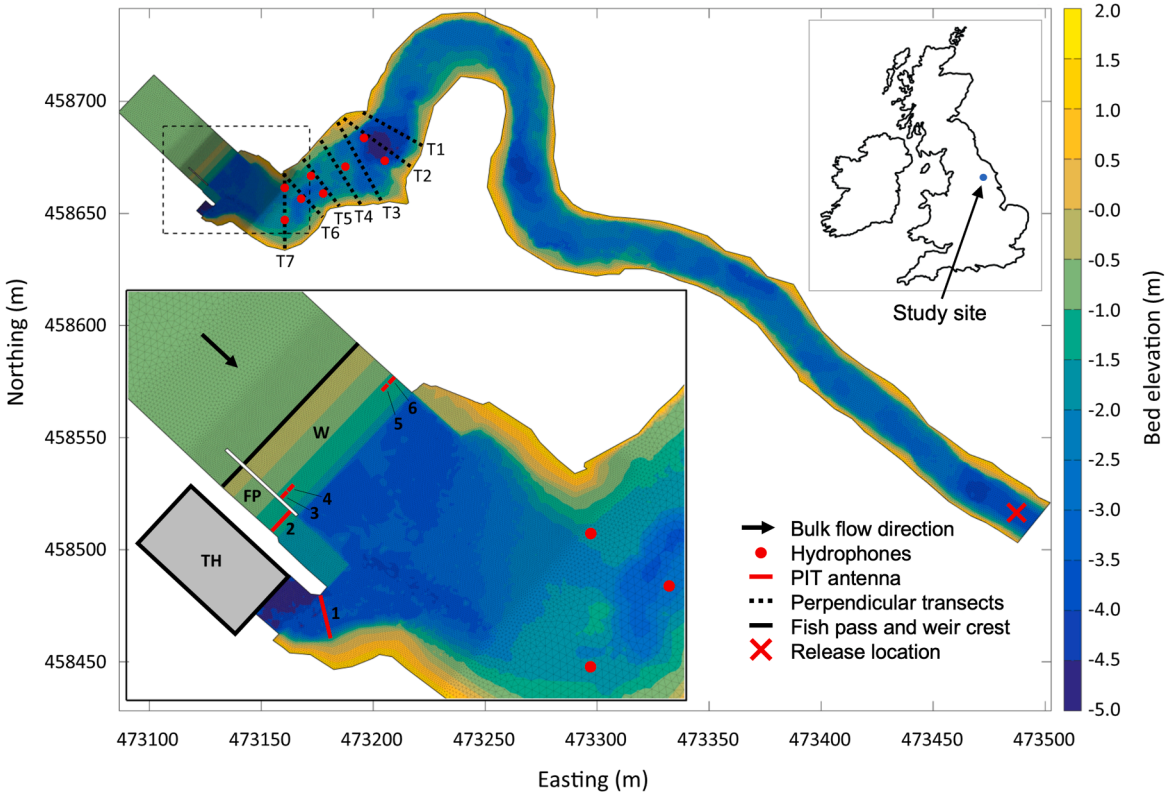

Fig. 1. Bed elevation (m) relative to weir crest of the 0.52 rkm reach downstream of the weir (W), fish pass (FP) and hydropower station (turbine house: TH), River Derwent, Yorkshire, UK. The triangular mesh grid used for the hydrodynamic models is overlaid. PIT antennas are 1: tailrace (TR), 2: fish pass (FP), 3: right bank bankside (RBB), 4: right bank mid-channel (RBM), 5: left bank mid-channel (LBM), 6: left bank bankside (LBB). Coordinate system: OSBG36.

hydrophones at mid-water depth on weighted vertical lines suspended from catenary ropes that spanned the width of the river (Fig. 1, Table S1) ensured that a test tag placed randomly within the array was detected by at least three receivers at all times. Placement of the array closer to the weir was not possible due to rapid attenuation of sound caused by high levels of air entrainment. Three-dimensional positioning was not possible because an undulating bathymetry and shallow water depth in key locations inhibited acoustic signal propagation. The hydrophones were connected to a model 290 HTI acoustic tag receiver (sample rate: 12 kHz) and a survey laptop running HTI AcousticTag data acquisition software.

Six PIT antennas were also installed on or near the weir to determine which routes the lamprey used as they attempted to pass upstream. PIT antennas function by generating a localised electromagnetic field which energises nearby tags, causing them to transmit a unique identification code, which is logged by a receiver. The antennas at the study site consisted of two pass-through type antennas, one in the tailrace and one at the downstream entrance of the fish pass and two pairs of flat-bed antennas at the foot of the weir, each pair covering a 2 m wide zone adjacent to the true right and left wing wall (Fig. 1). The antennas on the weir were the 'right bank bankside' (RBB), 'right bank mid-channel' (RBM), 'left bank mid-channel' (LBM) and 'left bank bankside' (LBB) (Fig. 1). The RBM antenna was located at the foot of a 1 m wide channel of studded tiles that were installed to aid lamprey passage (Tummers et al., 2018). The central 16 m of the weir was not instrumented. The acoustic and PIT telemetry equipment was operational at the site from 8 November to 7 December 2017 (30 days).

2.2.2. Lamprey capture and tagging

River lamprey were trapped near the tidal limit of the Ouse (latitude: 53.880002°, longitude: −1.1001047°, and at 53.885945°, −1.0959495°, WGS84) using double-compartment (two-funnel) eel pots (Masters et al., 2006) fishing on the riverbed. Over eight sessions between 8 - 29 November 2017, 34 lamprey (≥ 380 mm total length) were collected, transported to site, tagged and released at the downstream extent of the study area (Fig. 1, Table S2). Previous studies indicate that lamprey captured, tagged and released in this way are from the same genetic population (Bracken et al., 2015) and exhibit a consistent upstream-directed migration tendency (Lucas et al., 2009; Tummers et al., 2016b; 2018). Each lamprey was tagged intracoelomically with a 3.65 mm diameter × 32 mm long HDX PIT tag (Texas Instruments model RI-TRP-RRHP, 134.2 kHz, weight 0.8 g in air) and a 6.8 mm diameter × 20 mm long acoustic transmitter (HTISonar Model 795-LD, 307 kHz, weight 1.05 g in air). Acoustic transmitters were programmed to emit single acoustic pulses, with a variable pulse interval used to identify each tag (881–1182 ms). Lamprey moved upstream through the hydrophone array and approached the weir under a wide range of river flows (11.1-46.4 $m^3\ s^{-1}$). Due to a transcription error, PIT tag data for one lamprey was unavailable. All fish handling and tagging was conducted in compliance with UK Home Office Licence number PPL 70/8720 following the Animals (Scientific Procedures) Act 1986. See Tummers et al. (2018) for further details on lamprey capture, tagging and PIT telemetry.

2.2.3. Telemetry data processing

Acoustic telemetry data were processed using custom software written in Matlab R2017a (MathWorks). Tag positioning was undertaken in two stages: 1) an initial estimate of tag position was calculated based on *Time Difference of Arrival* (TDoA) of the signal between the three nearest hydrophones (intersection of hyperbola) and these positions were used to estimate the time each pulse was emitted from the tag (regression analysis); 2) *Time of Arrival* (ToA), the difference in signal transmit and receive time for the three nearest hydrophones, was used to calculate the final tag location (intersection of circles). TDoA and ToA

both produce multiple intersections reflecting both real and false potential detection locations. At each time step, during stage one and two, the clustered data points that most likely represented the real lamprey position were manually selected and averaged. As the focus of this study was to assess the movement dynamics of naïve lamprey as they approached a barrier, only their first upstream transit through the hydrophone array was tracked. To measure the spatial accuracy of the acoustic telemetry hardware and software, a transmitter (pulse interval: 1000 ms) was attached to a radio-controlled survey boat (ArcBoat) equipped with a high-precision global positioning system (see Section 2.3 for further details) and repeatedly driven through the hydrophone array (tag run). Tag runs were used to train the data analyst in the correct identification of real and false detection locations during tag positioning. The spatial accuracy of the system was validated by blind processing five randomly selected tag runs through the array (887 data points in total). This process revealed a median and maximum tracking error of 0.83 and 2.20 m, respectively. The location and time of first detection at the weir for each lamprey was extracted from the raw PIT telemetry data.

2.2.4. Analysis of movement patterns

Lamprey frequently held station (station holding behaviour) within the array for long periods. The frequency and duration that lamprey held station was quantified from the tracks as periods where they displayed cumulatively less lateral and longitudinal movement than the median acoustic tracking error (0.83 m) for $\geq$ 30 s. Transit time through the study area was subdivided into the duration: 1) between release and detection at the hydrophone array, 2) to pass through the array, and 3) between last acoustic detection and first PIT detection.

Lamprey lateral position across the channel was quantitatively assessed at seven transects (T1–7) spaced 10 m apart along the river centreline, oriented perpendicular to the primary flow direction (Fig. 1). The area between the most up and downstream transect conservatively spanned the domain in which it was possible to accurately position (acoustic telemetry) the lamprey as they moved upstream. Randomisation tests (Manly, 2007; Holbrook et al., 2015) were used to determine if lamprey lateral distribution was non-random at each transect. First, a random distribution (R) of locations was generated along each transect. To account for variable downstream water level during the study period, R for each transect was calculated by generating 1000 random intersect locations for each channel width available to each lamprey as it transited upstream, with all locations then aggregated. Second, the deviation between R and the observed distribution of lamprey (L) at each transect was established ($D_{R\text{-}L}$: Eq. (1)) by binning each distribution (R and L) into 10 equidistant bins and averaging the absolute difference between the proportion of L and R that occurred in each bin (i) (p_{Ri} and p_{Li}, respectively):

$$D_{R-L} = \frac{\sum |p_{Ri} - p_{Li}|}{10}. \quad (1)$$

Third, multiple ($n = 1000$) subsamples (R_s – number of positions per subsample equivalent to the observed number of lamprey) were randomly extracted from R, and the deviation between R_s and R ($D_{R\text{-}Rs}$) was calculated in the same way as between R and L (Eq. (1)). Finally, a p-value was calculated as the proportion of $D_{R\text{-}Rs}$ that were higher than $D_{R\text{-}L}$. For the randomisation tests, the p-value is a measure of the strength of evidence that lamprey lateral distribution was non-random, where $p < 0.01$, $p < 0.05$, $p < 0.10$, and $p > 0.10$ indicated strong, moderate, weak, and no evidence, respectively.

2.3. Hydrodynamic environment

Water velocity and bed elevation were measured downstream of the weir under mean flow conditions (discharge: 27.9 $m^3 s^{-1}$) using a radio-controlled survey boat (ArcBoat, L x W: 1.95 × 0.72 m), equipped with a Sontek RiverSurveyor M9 Acoustic Doppler Current Profiler (ADCP) and integrated Leica Viva GS14 Global Navigation Satellite System (horizontal position accuracy: 8 mm + 0.5 ppm). Raw ADCP data were processed using RiverSurveyor v4.0 (Sontek) to provide depth and velocity in three dimensions (x, y, and z) near the bed, surface and mid-column. Velocity magnitude was calculated from the three-dimensional flow vectors and averaged (mean) over all depths to produce depth averaged velocity and direction. Given the lack of knowledge about the vertical distribution of lamprey at the study site, depth averaged velocity was deemed to be the best approximation of the flow conditions they experienced. Bed elevation data were combined with wetted width, bank half-full and bank full measurements ($n = 493$), obtained using the Leica Viva GS14 attached to a 1.8 m survey pole, and linearly interpolated to produce a Digital Elevation Model (DEM) for the river channel downstream of the weir. Weir, fish pass and hydropower discharge and up- and downstream water level at the site were recorded at 15-minute intervals (Tummers et al., 2018).

Flow regimes experienced by the lamprey at times other than at mean discharge were modelled under nine conditions using five flows (11.1, 19.9, 28.8, 37.6 and 46.4 $m^3 s^{-1}$; hydrodynamic model: HM1–5, respectively) with the hydropower turbines either turned 'on' or 'off' (e.g. HM1_on and HM1_off) (Table S3). No 'turbine on' condition was needed for model HM5 as the head difference was low at this discharge and the hydropower station was not operational. The software used to model the hydrodynamics was TELEMAC-2D, which is a module of the open source TELEMAC-MASCARET modelling suite (www.opentelemac.org). It is acknowledged that there may have been significant vertical variation in flow at the study site but the lack of knowledge about lamprey distribution in this plane negated any potential benefits of undertaking more complex three-dimensional hydrodynamic modelling. The assumption of a two-dimensional environment is common in aquatic movement IBMs (Tan et al., 2018; Brosnan and Welch, 2020; Dye et al., 2022) and despite limitations can provide valuable insight into animal movement patterns. The model geometry, which consisted of an unstructured triangular mesh, was constructed using data derived from engineering drawings of the weir infrastructure and using the downstream channel DEM (Fig. 1). Model boundary conditions were parameterised using a constant value of water level at the downstream boundary and a constant discharge over the weir and through the fish pass and hydropower station. The individual discharge values used at each inflow boundary (e.g. through the fish pass) were derived from their measured relationship with total discharge when the turbines were either on or off (linear regression) (Figure S1, Table S3). Each of the nine hydrodynamic simulations were run with a computational timestep of 0.01 s and, to ensure model stability, the boundary conditions were applied gradually by linearly ramping the upstream boundary discharge from zero over a period of 12 h. The modelled hydrodynamic conditions were calibrated by comparing the output of model HM3_off (closest to mean discharge) with the ADCP data and the bed friction values of the model adjusted so that the gradient of the correlation between modelled and measured velocity closely matched (Figure S2). A spatially uniform Manning bed friction coefficient with a value of 0.045 $m^{1/3} s^{-1}$ was found to provide the best comparison. HM3_off produced comparable spatial flow patterns to those measured (Figure S3) and the root mean square error between the modelled and measured velocity along the reach was relatively low (0.19 m s^{-1}; Figure S2).

2.4. Pattern-oriented modelling (POM)

In this study, POM was used to identify the key hydrodynamic factors and fish behaviours that govern the movement patterns of upstream migrating lamprey as they approached an instream barrier. The POM approach involves the testing of multiple models of increasing complexity, including at least one 'null model' that is unrealistically simple (Grimm and Railsback, 2012). The reductionist process aims to derive the simplest model required to explain the movement patterns observed, incorporating only entities, variables and processes that are

absolutely essential (Grimm and Railsback, 2012). In this study, POM was achieved by: 1) identifying potentially important movement behaviours from the telemetry data obtained, 2) formulating multiple hypothetical movement models of increasing complexity based on the behaviours identified, 3) assessing each model's ability to reproduce the observed patterns (model performance), and 4) validating the model(s) that performed best. Each of these processes are explained in detail in Sections 2.4.1 to 2.4.4.

2.4.1. Identifying movement behaviour

Understanding of space use by riverine fish tends to reflect an interest in the relationship with flow (e.g. Goodwin et al., 2014; Kerr et al., 2016). Lamprey, however, exhibit quite different morphological and behavioural characteristics to many other fluvial species. For example, they lack paired fins that aid stability, and hold position in challenging flows (e.g. turbulent and high velocities) by attaching to hard surfaces with their oral disc (Kemp et al., 2009; Kerr et al., 2015). As a result, the relative importance of hydrodynamics compared to other variables, such as thigmotactic cues (Keefer et al., 2011; Kemp et al., 2011; Holbrook et al., 2015), remains difficult to ascertain. To identify the relative importance of hydrodynamics, lamprey movement models were created that were both independent and dependant of flow (See Section 2.4.2). To parameterise these models, lamprey movement behaviour was quantified from the acoustic telemetry lamprey tracks both independent (ground speed [G_{speed}] and direction [G_{dir}]) and dependant (swim speed [S_{speed}] and direction [S_{dir}]) of the hydrodynamic environment experienced. Assessment of movement behaviours for model parameterisation was undertaken using half of the acoustic telemetry tracks (parameterisation lamprey: $n = 16$) with the remainder used later to provide a 'within-site' validation of the model (validation lamprey: $n = 15$).

G_{speed} (m s^{-1}) and G_{dir} (°) at each time step were calculated as:

$$G_{speed} = \frac{\sqrt{(x_t - x_{t+1})^2 + (y_t - y_{t+1})^2}}{\delta t} \quad (2)$$

$$G_{dir} = atan2((x_t - x_{t+1}), (y_t - y_{t+1})) \quad (3)$$

where x and y are the Cartesian coordinates at time t and *atan2* is the four-quadrant inverse tangent in degrees [−180°, 180°]. A rotation was then applied so that G_{dir} was relative to the course of the river (upstream direction), which was calculated as the tangential angle of the river centreline at the point closest to the lamprey at that time step.

S_{speed} (m s^{-1}) and S_{dir} (°) were calculated as:

$$S_{speed} = \sqrt{(Su_t)^2 + (Sv_t)^2} \quad (4)$$

$$S_{dir} = atan2(Su_t, Sv_t) \quad (5)$$

where Su and Sv are the swim speeds (m s^{-1}) in x and y, extracted at each time step from each lamprey track as:

$$Su_t = (x_{t+1} - x_t)^* t - Fu_{(x_t, y_t)} \quad (6)$$

$$Sv_t = (y_{t+1} - y_t)^* t - Fv_{(x_t, y_t)} \quad (7)$$

where Fu and Fv are the flow velocities (m s^{-1}) in x and y at x and y, interpolated from the hydrodynamic model with the most appropriate discharge and turbine condition. Probability distributions were fitted to the movement variables G_{speed}, G_{dir}, S_{speed} and S_{dir} through assessment of log-likelihood scores. To assess whether lamprey movement was temporally autocorrelated, probability distributions of the difference between G_{speed}, G_{dir}, S_{speed} and S_{dir} between time steps were also evaluated (e.g. Eq. (8)).

$$G_{speeddiff} = G_{speed(t)} - G_{speed(t-1)} \quad (8)$$

The relationships between S_{speed} and S_{dir} and depth averaged flow speed (F_{speed}) and direction (F_{dir}) were investigated using regression analysis.

Broadscale trends in space use in relation to flow velocity and depth within the study area were evaluated using preference curves (P_V and P_D, respectively). Preference (P) was calculated as $P = U/A$, where U and A are histograms of space *used* and space *available*, respectively. The histograms were constructed by calculating the normalised frequency of U and V in the study area (between T1 and T7; Fig. 1) for increments (30 equally distributed bins) of either velocity or depth for each lamprey. *Available* velocity and depth consisted of all the data from the DEM (water level corrected) and from the most appropriate (nearest discharge and turbine condition) hydrodynamic model, respectively. *Used* velocity and depth was the interpolated values at each tracked lamprey position from the DEM and hydrodynamic models, respectively. Final preference curves were calculated as the mean and bootstrapped ($n = 1000$) confidence intervals (95%) of P for all individuals for each increment of the frequency distributions. When calculating preference as the quotient of use and availability, a fundamental assumption is that an organism has access to, and knowledge of, all space available to it, which is often not the case (Beyer et al., 2010). It is acknowledged that preference metrics which account for space 'sampled' are superior to those merely based on 'availability' (see Kerr et al., 2016). In this study, availability-based curves enabled efficient identification of broadscale distribution patterns relative to environmental variables and facilitated the generation of movement hypotheses that were later tested and validated as part of the POM process.

2.4.2. Movement models

Seven hypothetical movement models were formulated to predict the spatial-temporal distribution of upstream migrating river lamprey. These included four base level movement models of increasing complexity: Model 1) uniform spatial-temporal distribution (the null model); Model 2) flow independent random walk; Model 3) flow independent correlated random walk; and Model 4) flow dependant correlated random walk (Eulerian-Lagrangian model). In addition, the following three behavioural adaptations were made to the fourth model: avoidance of either a) shallow areas, b) slow flow areas, or c) shallow slow flow areas (Model 4a-c, respectively). Model 1 was a statistical model for which a uniform spatial and temporal distribution of lamprey was assumed (Table 1) and was formulated because the POM process requires inclusion of a simplistic null model against which to compare later models. Models 2–4c were spatially explicit IBMs in which agents moved through a hypothetical 2-dimensional domain representing the 0.52 rkm of channel downstream of the weir (Table 1). Agent movement in Models 2–4 was incorporated in different ways with later models being more complex. For example, in Models 2 and 3 movement behaviour was independent of local hydrodynamics and took the form of an uncorrelated and correlated random walk, respectively (Table 1). Models 2 and 3 were formulated to test whether adequate model fit could be achieved without using any hydrodynamics data, i.e. to ascertain whether lamprey movement might be independent of the flow field. Model 4 was a coupled Eulerian-Lagrangian model in which agents were advected downstream with the flow, and movement was the result of swim- and flow- speed and direction in two dimensions (Table 1). Model 4 was formulated to test how important local hydrodynamics are for governing lamprey movement. The addition of extra movement behaviours in Models 4a-c (e.g. addition of avoidance of shallow and/or slow flow regions) increased model complexity further but enabled systematic testing of each behaviour in relation to the base model (Model 4). Models 2–4c had a timestep of 1 second and were parameterised using the data generated in Section 2.4.1.

For Models 2–4c, agents were released into the model at the downstream extent of the domain (Fig. 1) and movement occurred at each time step according to user defined rules. Agents were kept within the domain boundaries through checks that occurred at each time step. If

Table 1
Details of each of the seven movement models that were formulated to predict the spatial-temporal distribution of upstream migrating river lamprey.

Model	Model type		Hydrodynamics		Movement type		Avoidance behaviour	
	Statistical	Spatially explicit IBM	Independent	Dependant	Random walk	Correlated random walk	No	Yes
1	x		x		N/A		x	
2		x	x		x		x	
3		x	x			x	x	
4		x		x		x	x	
4a		x		x		x		x ($D <= 1$)
4b		x		x		x		x ($V <= 0.1$)
4c		x		x		x		x ($D <= 1$ & $V <= 0.1$)

D: Depth (m)
V: Depth averaged velocity (m s^{-1})

the agent's next movement was determined to place it outside of the model boundary, then a hypothetical selection of twenty alternative movement locations were generated that fell on the perimeter of a circle centred on the last movement position and with a radius (r) equal to current step length. Of these hypothetical points, the one that was closest to the erroneous position that was within, and did not cross the model boundary, was selected as the new movement location. This method enabled continuation of the agent's movement in a direction

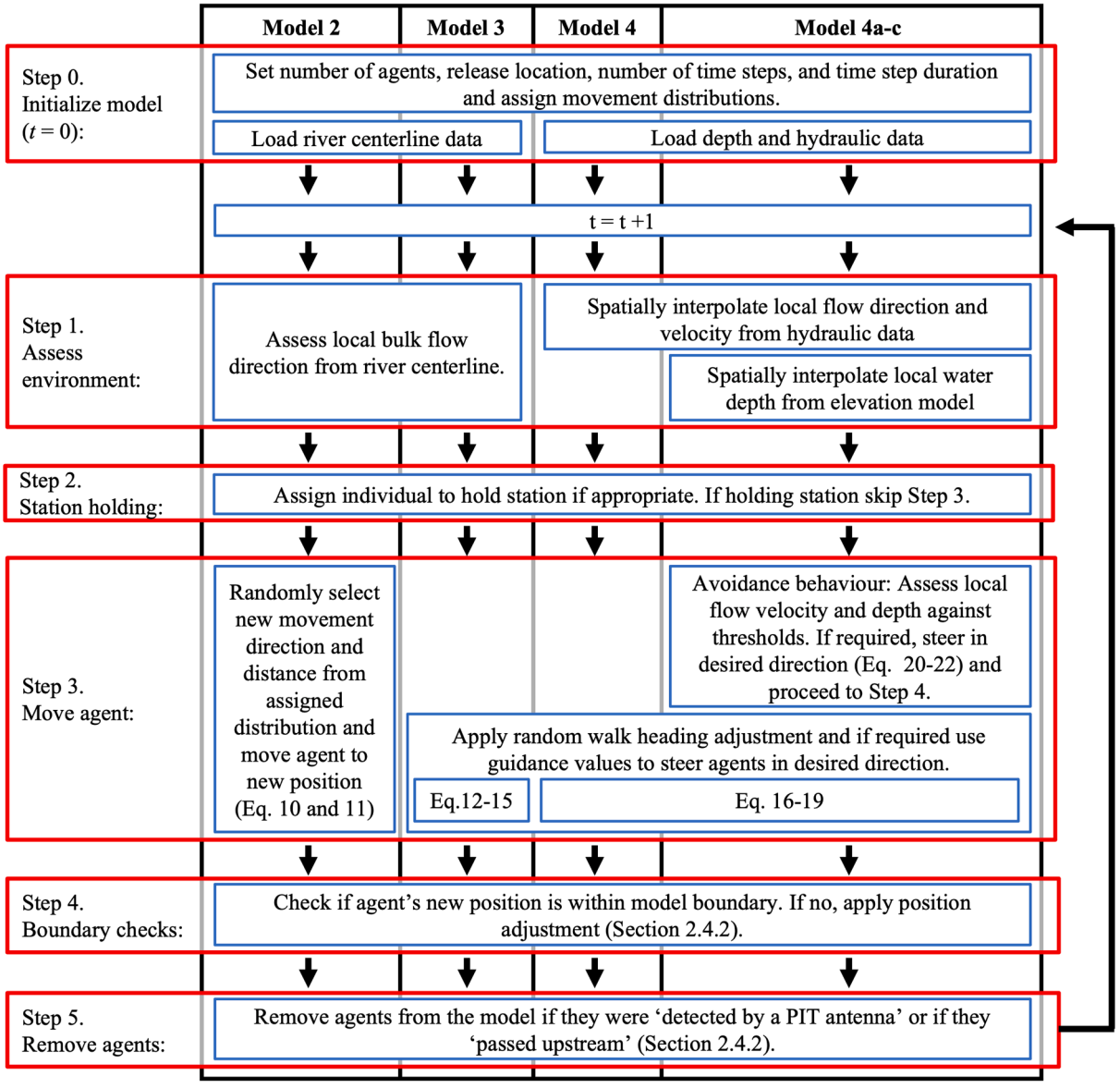

Fig. 2. Flow diagram of the Individual Based Models (2–4c) used to predict the upstream movement of European river lamprey as they approached an instream barrier. Workflow for each Model (2–4c) is contained within each black rectangle and should be read from top to bottom. Red boxes outline the six major processes common to each of the models. Internal blue boxes outline processes specific to each model. If all or part of a blue box is within a black rectangle then that process is part of the model. Further details for each model can be found in Sections 2.4.2.2 – 2.4.2.5.

similar to its 'intended' movement direction and maintained the predetermined movement distance for that time step (Benson et al., 2021).

Station holding was implemented into Models 2–4c by assigning a probability ($P_{SH} = 0.00299$) that each agent would exhibit this behaviour at each time step. P_{SH} was calculated as:

$$P_{SH} = 1 - \left(1 - \left(\frac{N_{SH}}{n}\right)\right)^{(1/\mu_{TL})} \quad (9)$$

where, N_{SH} is the number of lamprey that held station, n is the number of lamprey observed and μ_{TL} is the mean tracking duration. When initiated, the agent held station for a set number of time steps, randomly assigned from a distribution (logistic, $\mu = 17.8$, $\sigma = 28.1$, truncation: 0, 801) fitted to the empirical data (Figure S4). Turbulence was simulated in Model 4 and sub models by randomly varying *Fu* and *Fv* by a factor of $R\{N(Fu,\ 0.2)\}$ and $R\{N(Fv,\ 0.2)\}$, respectively, where R{X} is a random number from the distribution X and $N(\mu,\ \sigma)$ is a normal distribution with mean μ and standard deviation σ. Agents were removed from the model if they crossed user-selected detection lines set at the PIT antenna locations and at the crest of the fish pass and weir (Fig. 1). As such, agents were removed from the model if they were 'detected by a PIT antenna' or if they 'passed upstream'.

Changing flow conditions (e.g. discharge and water depth) during the study period (Figure S5) were accounted for in Models 2–4c by weighting the number of agents 'released' in each hydrodynamic model. One thousand agents were released per lamprey, which provided an appropriate balance between limiting model run time and ensuring emergent patterns were fully resolved (i.e. sufficient replicates to overcome model stochasticity). For example, for the parameterisation lamprey, the number of agents that best represented the different flow conditions experienced (matching turbine condition and nearest discharge) was 4000, 5000, 2000, 3000 and 2000 released using the HM1_off, HM1_on, HM2_on, HM4_off and HM5_off, hydrodynamic model data, respectively (16,000 in total). This process resulted in the proportion of agents and lamprey that experienced different flow conditions being comparable. When assessing the results against the 'validation' or 'all' lamprey, the models were rerun with the appropriate number of agents to ensure comparability. Further details for each model are provided in the subsections below. For the IBMs (Models 2–4c), model processes are summarised in a flow chart in Fig. 2.

2.4.2.1. Model 1 - Uniform spatial-temporal distribution. Model 1 was a statistical model for which a uniform spatial and temporal distribution of lamprey was assumed. To account for the variable channel width throughout the study period and to ensure that the assumed distribution was comparable to that observed, a uniform lateral distribution at each transect (T1-T7) was calculated for the wetted width available to each lamprey as they migrated upstream (extrapolated from the DEM and downstream water level) and the results aggregated (i.e. a weighted uniform distribution). The time taken for agents to transit through the hydrophone array and their first PIT detection locations were assumed to be uniformly distributed, with no weighting applied.

2.4.2.2. Model 2 - Flow independent random walk. Model 2 was a biased random walk model (e.g. Codling et al., 2008) in which agents moved through the domain independent of the hydrodynamic environment. The agents were guided by river geometry (course of the river extracted from the centreline) with values of ground speed and direction at each timestep randomly allocated from the observed probability distributions of each (pd_G_{speed} and pd_G_{dir}, respectively) (Table 2, Figure S6). Movement in x and y at each timestep (t) was calculated as:

$$x_{(t)} = x_{(t-1)} + cos\left(R\{pd\_G_{dir}\}\right)*R\{pd\_G_{speed}\}*t \quad (10)$$

$$y_{(t)} = y_{(t-1)} + sin\left(R\{pd\_G_{dir}\}\right)*R\{pd\_G_{speed}\}*t \quad (11)$$

2.4.2.3. Model 3 – Flow independent correlated random walk. Model 3 was similar to Model 2 in that agents moved through the domain independent of the hydrodynamic environment. However, movement (G_{speed} and G_{dir}) at each time step was temporally autocorrelated. Initial agent G_{speed} and G_{dir} values were randomly selected from the pd_G_{speed} and pd_G_{dir} distributions (Table 2, Figure S6) as per for Model 2. Subsequent G_{speed} and G_{dir} values were assigned to agents as:

$$G_{speed(t)} = G_{speed(t-1)} \pm R\{pd\_G_{speeddiff}\} \quad (12)$$

$$G_{dir(t)} = G_{dir(t-1)} \pm R\{pd\_G_{dirdiff}\} \quad (13)$$

where $pd\_G_{speeddiff}$ and $pd\_G_{dirdiff}$ are the probability distributions of observed difference in either G_{speed} or G_{dir} between each time step, respectively (Table 2, Figure S6). To keep the agents moving at an appropriate speed and heading in the correct direction, current G_{speed} and G_{dir} values were periodically assessed against a randomly selected value from the observed probability distributions of each (guidance values) (Table 2). Whether the current value was greater or lesser than the guidance value determined if the change in the movement parameter for that time step was subtracted or added, respectively (G_{speed}: Eq. (14); G_{dir}: Eq. (15)).

$$\begin{aligned} G_{speed(t)} < R\{pd\_G_{speed}\} &\rightarrow G_{speed(t)} = G_{speed(t-1)} + R\{pd\_G_{speeddiff}\} \\ G_{speed(t)} \geq R\{pd\_G_{speed}\} &\rightarrow G_{speed(t)} = G_{speed(t-1)} - R\{pd\_G_{speeddiff}\} \end{aligned} \quad (14)$$

$$\begin{aligned} G_{dir(t)} < R\{pd\_G_{dir}\} &\rightarrow G_{dir(t)} = G_{dir(t-1)} + R\{pd\_G_{dirdiff}\} \\ G_{dir(t)} \geq R\{pd\_G_{dir}\} &\rightarrow G_{dir(t)} = G_{dir(t-1)} - R\{pd\_G_{dirdiff}\} \end{aligned} \quad (15)$$

As such, for each agent, the deviation of G_{speed} and G_{dir} values

Table 2
Probability distributions of the movement variables, extracted from the 16 parameterisation lamprey, used in the spatially explicit IBMs (Models 2–4c).

Movement distribution	Distribution type	Units	Distribution parameters	Distribution truncation	Used in Model
pd_G_{speed}	Generalized Extreme Value	m s^{-1}	$k = 0.1183$, $\sigma = 0.1708$, $\mu = 0.2361$	0, 4.75	2, 3
pd_G_{dir}	Normal	degrees	$\mu = 2.3654$, $\sigma = 67.3824$	−180, 180	2, 3
$pd\_G_{speeddiff}$	Exponential	m s^{-1}	$\mu = 0.1254$	0, 4.60	3
$pd\_G_{dirdiff}$	Exponential	degrees	$\mu = 31.4790$	0, 180	3
$pd\_LF\_S_{speed}$	Burr	m s^{-1}	$\alpha = 4.6984$, $c = 1.6135$, $k = 44.8536$	0, 1.41	4, 4a, 4b, 4c
$pd\_LF\_S_{dir}$	Uniform	degrees	lower = 0, upper = 180	0, 180	4, 4a, 4b, 4c
$pd\_LF\_S_{speeddiff}$	Exponential	m s^{-1}	$\mu = 0.1296$	0, 0.8974	4, 4a, 4b, 4c
$pd\_LF\_S_{dirdiff}$	Exponential	degrees	$\mu = 35.8540$	0, 180	4, 4a, 4b, 4c
$pd\_MHF\_S_{speed}$	Generalized Extreme Value	m s^{-1}	$k = -0.0335$, $\sigma = 0.2138$, $\mu = -0.1086$	−0.96, 4.45	4, 4a, 4b, 4c
$pd\_MHF\_S_{dir}$	Exponential	degrees	$\mu = 16.4706$	0, 180	4, 4a, 4b, 4c
$pd\_MHF\_S_{speeddiff}$	Exponential	m s^{-1}	$\mu = 0.1144$	0, 4.91	4, 4a, 4b, 4c
$pd\_MHF\_S_{dirdiff}$	Exponential	Degrees	$\mu = 10.9685$	0, 180	4, 4a, 4b, 4c

pd: probability distribution; G_{speed}: ground speed; G_{dir}: direction (relative to river course); $G_{speeddiff}$: ground speed difference between timesteps; $G_{dirdiff}$: direction difference between timesteps; LF: low flow swimming behaviour; MHF: moderate to high flow swimming behaviour; S_{speed}: swim speed; S_{dir}: swim direction (relative to flow direction); $S_{speeddiff}$: swim speed difference between timesteps; $S_{dirdiff}$: swim direction difference between timesteps.

between timesteps followed the pd_$G_{speeddiff}$ and pd_$G_{dirdiff}$ distributions and the direction of change was periodically adjusted to guide fish in accordance with the pd_G_{speed} and pd_G_{dir} distributions. As applying guidance every time step resulted in overly persistent agent movement paths, the probability that it was applied (P_{speed} and P_{dir} for G_{speed} and G_{dir}, respectively) was iteratively adjusted until agent movement distance and direction distributions matched those observed ($P_{dist} = 0.94$; $P_{dir} = 0.75$).

2.4.2.4. Model 4 – Flow dependant correlated random walk. In Model 4, agent movement was dependant on hydrodynamics and the result of both swim and flow speed and direction in two dimensions. That is, agents had to actively swim against the flow to hold position or make progress upstream. Two different swimming behaviours in response to flow velocity were identified from assessment of the telemetry and hydrodynamic data (Fig. 3a) and incorporated in Model 4. These were: 1) low flow swimming ($F_{speed} < 0.1$ m s^{-1}) and 2) moderate to high flow swimming ($F_{speed} \geq 0.1$ m s^{-1}) behaviours. During low flow swimming ($F_{speed} < 0.1$ m s^{-1}), swim direction was independent of flow direction and movement paths were relatively tortuous (Figure S7). During moderate to high flow swimming ($F_{speed} \geq 0.1$ m s^{-1}), lamprey tended to swim against the flow, swim speed was correlated with flow velocity, and movement was more persistent (Figure S8). Movement dynamics (e.g. S_{speed} and S_{dir}) within Model 4 were calculated in the same way for both the low flow and moderate to high flow swimming behaviours but values were randomly drawn from different probability distributions (e.g. pd_LF_S_{speed} and pd_MHF_S_{speed}, respectively: Table 2).

Guidance to keep the agents following observed swim speed and direction distributions was applied in the similar way as in Model 3, with the same probability of guidance at each time step ($P_{speed} = 0.94$; $P_{dir} = 0.75$). Initial S_{speed} and S_{dir} values were randomly selected from the observed pd_S_{speed} and pd_S_{dir} distributions (Table 2). The best distribution fit for the pd_LF_S_{dir} and pd_MHF_S_{dir} data occurred when absolute values were used (hence the distribution is limited to between 0 and 180° in Table 2). When required, values generated using these distributions were multiplied by either −1 or 1 (randomly selected) to enable a full range of possible turn angles (i.e. final distribution truncation: −180°, 180°). Subsequent S_{dir} values were assigned to agents as:

$$\begin{aligned} S_{dir(t)} &< R\{pd\_S_{dir}\} \rightarrow S_{dir(t)} = S_{dir(t-1)} + R\{pd\_S_{dirdiff}\} \\ S_{dir(t)} &\geq R\{pd\_S_{dir}\} \rightarrow S_{dir(t)} = S_{dir(t-1)} - R\{pd\_S_{dirdiff}\} \end{aligned} \quad (16)$$

To account for a linear relationship between S_{speed} and F_{speed}, S_{speed} values were assigned to agents as:

$$\begin{aligned} S_{speed(t)} &< aF_{speed} + b + R\{pd\_S_{speed}\} \rightarrow S_{speed(t)} = S_{speed(t-1)} + R\{pd\_S_{speeddiff}\} \\ S_{speed(t)} &\geq aF_{speed} + b + R\{pd\_S_{speed}\} \rightarrow S_{speed(t)} = S_{speed(t-1)} - R\{pd\_S_{speeddiff}\} \end{aligned} \quad (17)$$

Where a and b are the slope and intercept, respectively, of the linear relationship between flow and swim speed identified from the analysis described in Section 2.4.1 (Fig. 3b). Values of a and b in Eq. (17) were zero during low flow swimming (Figure S7) and 0.75 and 0.40, respectively, during moderate to high flow swimming (Figure S8). Agent movement in x in y was calculated as:

$$x_{(t)} = x_{(t-1)} + ((Fu + R\{N(Fu, 0.2)\}) * t) + (cos(S_{dir}) * S_{speed} * t) \quad (18)$$

$$y_{(t)} = y_{(t-1)} + ((Fv + R\{N(Fv, 0.2)\}) * t) + (sin(S_{dir}) * S_{speed} * t) \quad (19)$$

2.4.2.5. Models 4a-c. Assessment of the depth and velocity preference curves for the parameterisation lamprey indicated that they moved through shallow and slow flow regions less frequently than expected if their distribution had been uniform throughout the study area (Figure S9). To evaluate whether avoidance of these regions might be influencing space use, three additional movement behaviours were added to Model 4: avoidance of either shallow areas (Model 4a), slow flow areas (Model 4b), or shallow slow flow areas (Model 4c). Depth and velocity avoidance thresholds (D_{avoid} and V_{avoid}, respectively) were set at 1 m and 0.1 m s^{-1}, respectively. At each time step, depth and velocity at the agent's location (A_{depth} and $A_{velocity}$, respectively) were interpolated from the hydrodynamic model. If $A_{depth} < D_{avoid}$ (Model 4a), $A_{velocity} < V_{avoid}$ (Model 4b) or $A_{depth} < D_{avoid}$ and $A_{velocity} < V_{avoid}$ (Model 4c) then avoidance behaviour was initiated. Avoidance behaviour superseded all other movement behaviours and consisted of the fish moving towards deeper (Model 4a and 4c) or higher velocity (Model 4b) areas. Gradients of increasing depth ($\theta_{\nabla d}$) and velocity ($\theta_{\nabla v}$) were calculated for each hydrodynamic model (Eqs. (20) and (21), respectively) and interpolated at each agent position as required.

$$\theta_{\nabla d} = atan2\left(\frac{\partial d}{\partial x}, \frac{\partial d}{\partial y}\right) \quad (20)$$

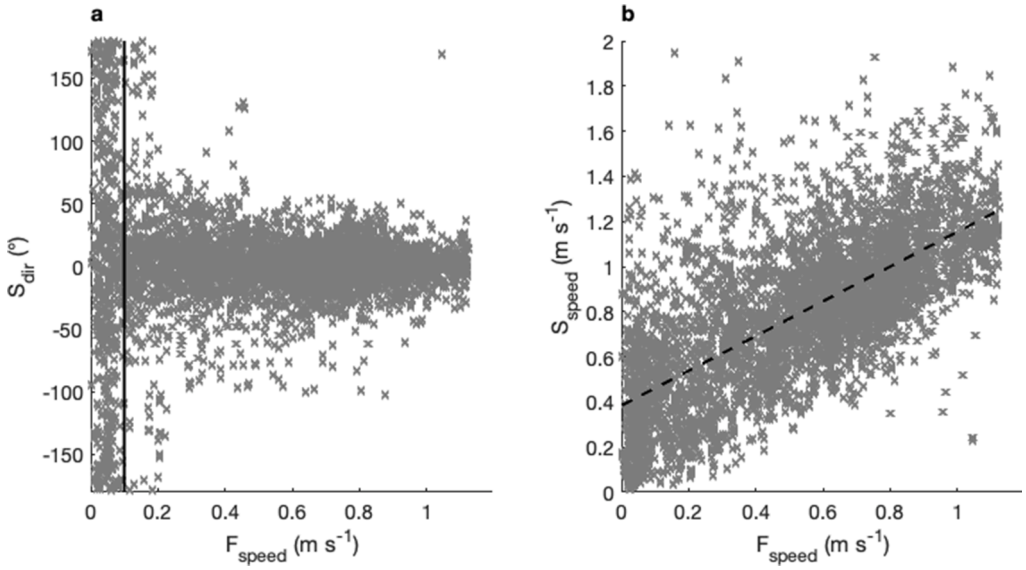

Fig. 3. Relationship between flow speed (F_{speed}) and a) swim direction (S_{dir}) and b) swim speed (S_{speed}) for the parameterisation lamprey as they transited upstream though the hydrophone array and approached Buttercrambe weir, Yorkshire, UK. The solid black line represents the flow speed cut-off threshold ($F_{speed} = 0.1$ m s^{-1}) between the identified low flow and moderate to high flow swimming behaviours; the dashed line is the fitted linear relationship between F_{speed} and S_{speed}.

$$\theta_{\nabla v} = atan2\left(\frac{\partial v}{\partial x}, \frac{\partial v}{\partial y}\right) \quad (21)$$

Steering towards $\theta_{\nabla d}$ and $\theta_{\nabla v}$ occurred by adding or subtracting a random change in bearing from the distribution pd_$S_{dirdiff}$ (Table 2). For example, for Model 4a if avoidance behaviour was initiated then Eq. (22) was applied:

$$\begin{aligned} S_{dir(t)} < \theta_{\nabla d(t)} \rightarrow S_{dir(t)} &= S_{dir(t-1)} + R\left\{pd\_S_{dirdiff}\right\} \\ S_{dir(t)} \geq \theta_{\nabla d(t)} \rightarrow S_{dir(t)} &= S_{dir(t-1)} - R\left\{pd\_S_{dirdiff}\right\} \end{aligned} \quad (22)$$

During avoidance behaviour, agents therefore steered away from either shallow and/or slow flow regions in the direction (left or right) that most closely aligned them with increasing velocity or depth, but their turn angles continued to adhere to pd_$S_{dirdiff}$. Agents displaying avoidance behaviour might not immediately exit an undesirable region (e.g. shallow water) but the behaviour typically resulted in them spending less time in such areas.

2.4.3. Model performance

The accuracy with which each of the seven models predicted the observed patterns exhibited by the parameterisation lamprey was quantified in terms of the mean absolute difference between simulated and empirical probability distributions. This was achieved using three distributions: 1) lamprey lateral position across the river at each of the seven perpendicular transects (lateral deviation), 2) upstream passage time between transect T1 and T7 (temporal deviation), and 3) location of first PIT detection (PIT deviation). For each deviation score (lateral, temporal and PIT), the probability distributions were standardised to ensure comparability between observed and modelled data. For lateral deviation, 10 equally spaced bins of normalised lateral position (0 to 1, from left to right bank) along each transect (widest wetted width available) were used. For temporal deviation, 10 equally spaced bins between zero and the maximum time (seconds) taken for a lamprey to pass through the hydrophone array (excluding outliers: > 2000 s) were used. For PIT deviation, eight sampling locations were used: 1–6) the first PIT detection location after passing upstream through the acoustic array (TR, FP, RBB, RBM, LBM or LBB), 7) 'passed upstream', and 8) 'not detected'. Raw and normalised lateral, temporal and PIT deviation scores were calculated for each model (1–4c) and ranked. Normalised scores were calculated relative to the null model (0) and the best performing model (1), with models that performed worse than the null model attributed negative values. Combined overall model predictive performance was assessed as the normalised and ranked mean of the lateral, temporal and PIT deviation scores.

2.4.4. Model validation

Models were validated by assessing their ability to predict the spatial-temporal distribution of the validation lamprey ($n = 15$) telemetry tracks that had been excluded from the parameterisation process. As sample size for parameterisation and validation were similar, the deviation scores generated from the models were comparable. A final assessment of the best model(s) was undertaken by comparing the percentage error (deviation score × 100) in the predicted lateral, temporal and PIT distributions compared to the null model (Model 1: uniform spatial, temporal and PIT distribution) for all lamprey telemetry tracks ($n = 31$).

3. Results

3.1. Movement patterns

Of the 34 tagged lamprey released, 32 were detected and 31 progressed upstream through the acoustic array. The median time taken to reach the array after release was 78.2 min (range: 26.1 min-10.2 days). The median time taken to pass through the array was 5.8 min (range: 2.8 min-10.1 days). Lamprey movement through the array was tortuous (Fig. 4a), and their lateral distribution across the channel non-random at T2 and T3 ($p < 0.05$) (Fig. 4). During their first upstream transit, most lamprey held station at least once (median frequency: 1; range: 0–17) for a median duration of 1.3 min (range: 30 s-10.1 days). After passing upstream through the array for the first time, 53% of lamprey ($n = 16$)

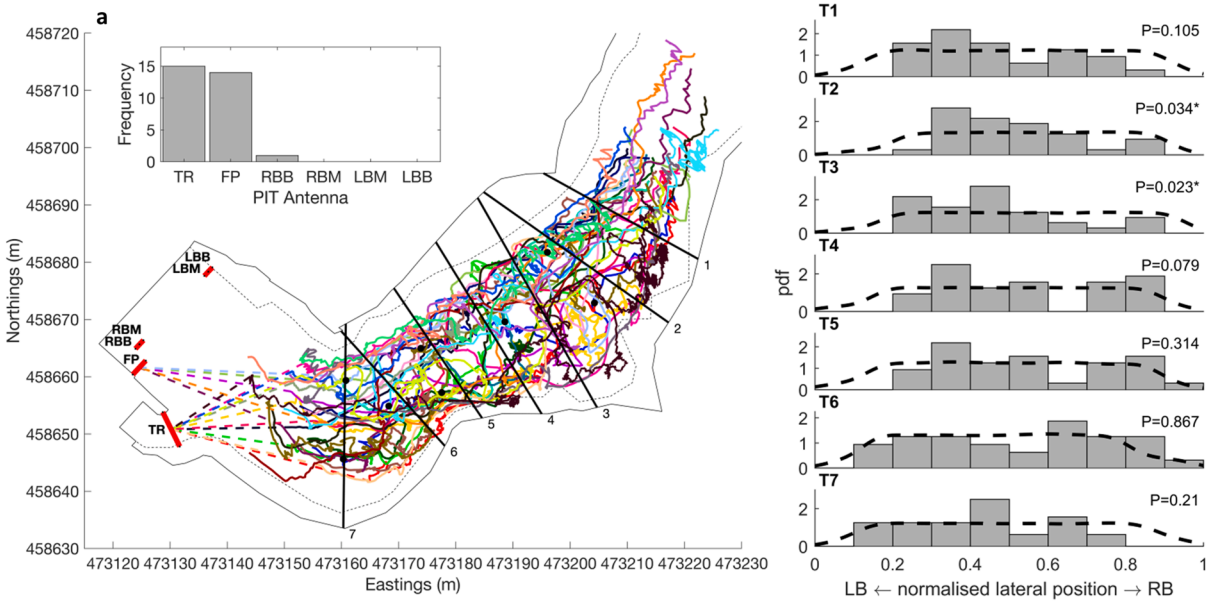

Fig. 4. Acoustic telemetry tracks of upstream moving river lamprey ($n = 31$) (solid coloured lines) (a) and their normalised lateral distributions (grey bars) as they transited upstream through perpendicular transects T1–7 and approached a Crump weir and hydropower station (T1–7). For a, solid and dashed thin black line are the bank full boundary and wetted width at discharge = 18.7 m^3 s^{-1}, respectively; thick black lines are transects T1-T7; dashed coloured lines link the last acoustic detection and first PIT detection for the 53% ($n = 16$) of lamprey that were immediately detected at the weir infrastructure; red rectangles bounded by small black dots represent PIT antenna locations; inset figure is histogram of first detection location for all PIT detected lamprey ($n = 30$). For T1–7, inset p values < 0.05 indicate the lamprey lateral distribution was significantly different from random (dashed black line). LB and RB are Left and Right Bank, respectively. Coordinate system: OSBG36.

were next detected at one of the PIT antennas (Fig. 4a). For these, the median duration between last acoustic and first PIT detection was 10.7 min (range: 0.4–51.8 min). The remaining lamprey (47%) transited back into, or progressed downstream beyond, the array prior to detection at one of the PIT antennas. First PIT detections for all PIT tagged lamprey that passed upstream through the array (n = 30) predominantly occurred at the bottom of the fish pass (50%) or within the hydropower tailrace (47%) (Fig. 4a).

3.2. Hydrodynamic environment

Mean wetted width, velocity and depth respectively ranged from 23.4 to 31.8 m, 0.34 to 0.46 m s^{-1} and 0.9 to 2.3 m between low (11.1 m^3 s^{-1}) and high (46.4 m^3 s^{-1}) discharge (Fig. 5a and b, respectively). Hydrodynamic conditions varied considerably between transects (Fig. 5 T1–7), e.g. at 11.1 m^3 s^{-1} mean velocity was highest at T5 (0.60 m s^{-1}; range: 0.04–0.88), and lowest at T2 (0.14 m s^{-1}; range: 0.01–0.38) (Fig. 5 T1–7), while mean depth was highest at T2 (3.21 m; range: 0.59–3.92) and lowest at T7 (0.67 m; range: 0.00–1.30) (Fig. 5 T1–7). Five of the seven transects featured areas of flow recirculation adjacent to one (T1, T2, T4, and T6) or both (T2) banks (Fig. 5 T1–7). At T2 and T3, the transects at which lamprey distribution was non-random, flow recirculation accounted for more than 30% of the channel width (Fig. 5 T2, T3). Areas of recirculation occurred at all discharges, particularly near the right bank at T2 and T3 (Fig. 5).

3.3. Pattern-oriented modelling (POM)

Out of the base models, Model 4 and Model 2 were the best and worst predictors of lamprey lateral distribution, respectively (Figs. 6 and 7, Table 3). Movement trajectories of agents produced by Model 2 (Fig. 6a) were more persistent than those observed (Fig. 4a), and as the agents migrated upstream around each bend they tended to aggregate, resulting in an uneven distribution across the channel (Fig. 7). Lateral

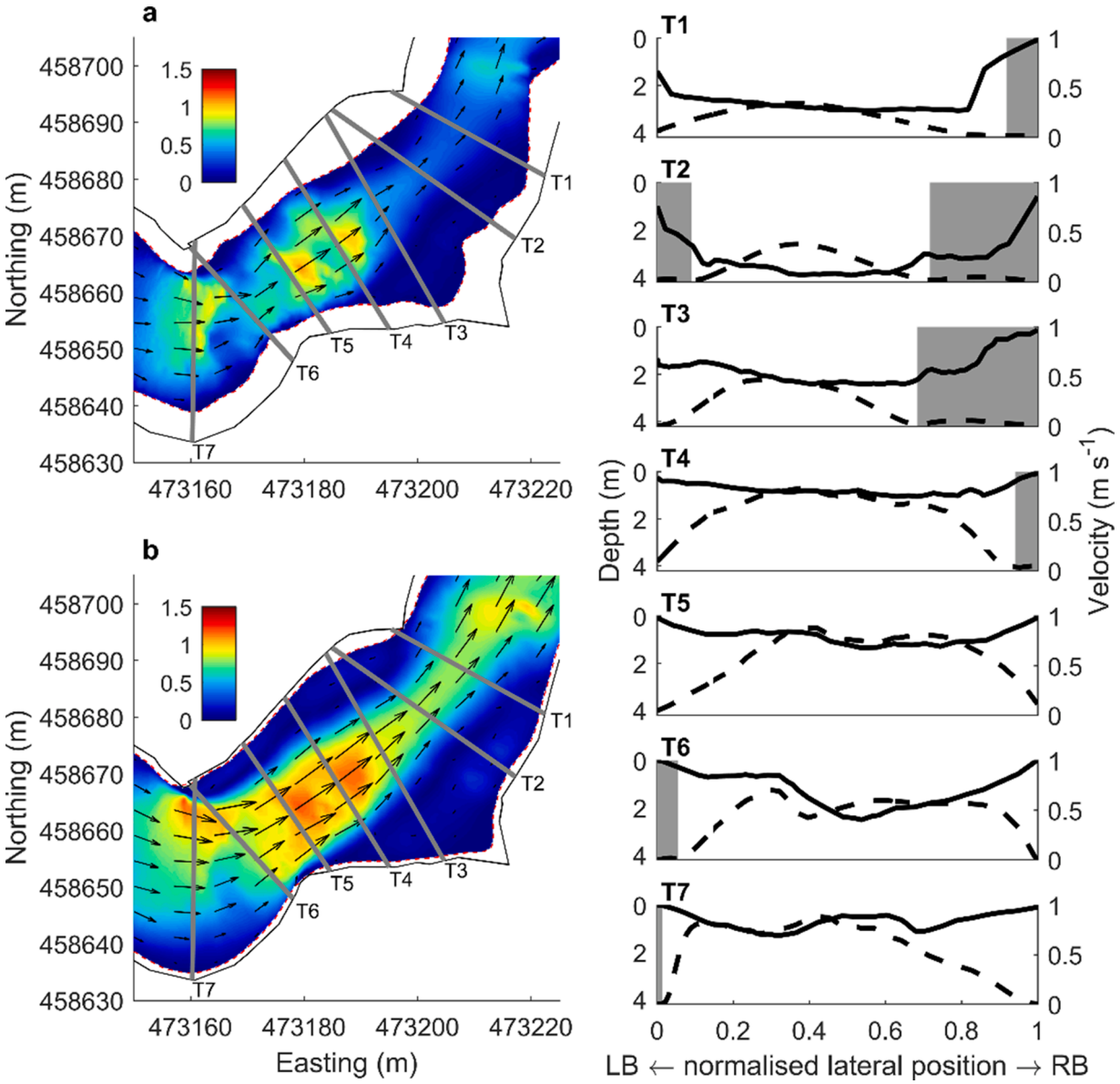

Fig. 5. Maps of depth averaged velocity (V: m s^{-1}) for the hydrodynamic model M1_off (a) and M5_off (b) showing the changing flow conditions and wetted widths at low and high discharge, respectively. Black arrows are velocity vectors. The thin black line is the bank full boundary. Grey lines (T1–7) are the perpendicular transects at which lamprey lateral distribution was assessed. Coordinate system: OSBG36. Subplots T1–7 show water depth (m) (left axis, solid line) and depth averaged velocity (m s^{-1}) (right axis, dashed line) along each transect (normalised lateral position from left [LB] to right [RB] bank) for hydrodynamic model M1_off (discharge: 11.1 m^3 s^{-1}). Shaded regions highlight areas of flow recirculation (areas where flow direction is > 90° from the bulk flow direction).

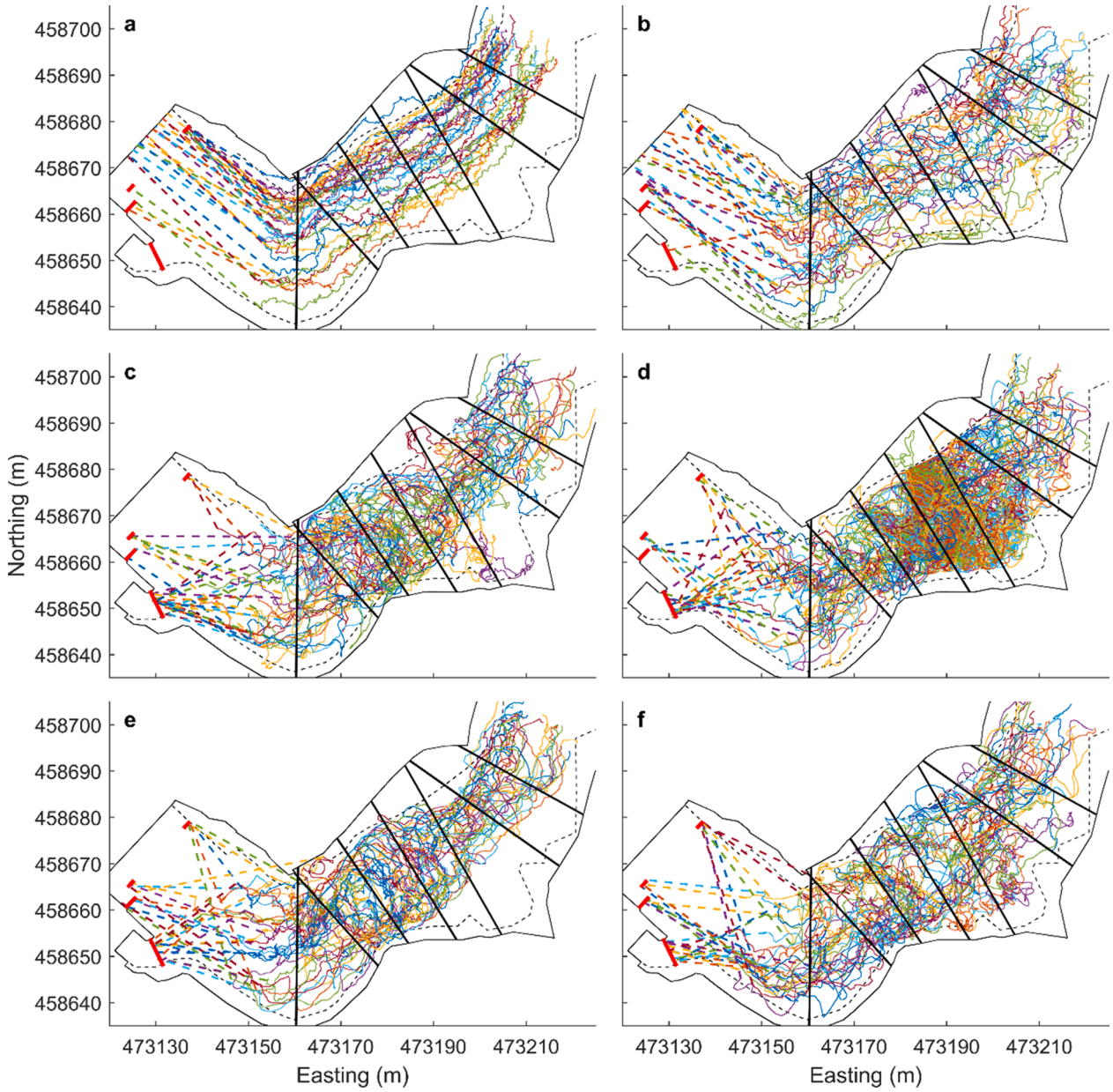

Fig. 6. Movement paths ($n = 31$) predicted by a) Model 2, b) Model 3, c) Model 4, d) Model 4a, e) Model 4b, and f) Model 4c. Solid coloured lines are the predicted paths through the hydrophone array. Dashed coloured lines link the agent location 40 s after passing through Transect 7 to the first PIT antenna (red lines) detection or where they passed the weir crest. Thick black lines are the transects (T1–7) used to assess lamprey lateral distribution. Solid and dashed thin black lines are the bank full channel boundary and wetted width at discharge = 18.7 m^3 s^{-1}, respectively. Coordinate system: OSBG36.

distributions produced in Model 4, matched those of lamprey well (Fig. 7), resulting in the lowest deviation score for the base models (Table 3). The addition of avoidance behaviours in Model 4a and Model 4b resulted in poorer prediction of lateral distributions than the base model alone (Table 3). Model 4c, which included avoidance of shallow slow flow regions, was the best model overall for predicting lateral distribution of lamprey (Table 3).

Median time taken for lamprey to pass through the array was 327 s with a few individuals taking longer (up to 1800 s) (Fig. 8a). Out of the base models, Model 1 was the poorest predictor of time to pass (Fig. 8a; Table 3). Model 3 was the best, closely followed by Model 4 (Fig. 8a; Table 3), with predicted median agent durations of 349 and 364 s, respectively. The more persistent movement paths produced by Model 2 (Fig. 6a) resulted in less variation in passage time and a greater peak in the distribution around the median value (324 s) (Fig. 8a). The addition of avoidance behaviours in Model 4a and Model 4b resulted in a poorer prediction of passage time than the base model alone (Table 3). Model 4a was particularly bad at predicting passage time (Fig. 8a; Table 3) as avoidance of shallow regions around transect T4 (Fig. 6d) delayed agent upstream progress. Model 4c, which included avoidance of shallow slow flow regions, provided the best predictions of lamprey temporal distribution overall (Fig. 8a; Table 3).

For the parameterisation lamprey that were immediately detected at a PIT antenna after transiting upstream through the hydrophone array ($n = 7$ lamprey), the majority of detections (57%) occurred at the tail-race, followed by the fish pass (43%) (Fig. 8b). Models 2 and 3 were particularly poor at predicting first PIT antenna detections (Fig. 8b; Table 3) because there was no underlying hydrodynamic feedback to stop the agents 'passing' upstream over the high velocity flows that occur on the weir face (Fig. 6a and b), whereas Model 4 was the most predictive (Fig. 8b; Table 3). None of the additional avoidance behaviour models (4a-4c) improved PIT detection predictions compared to the

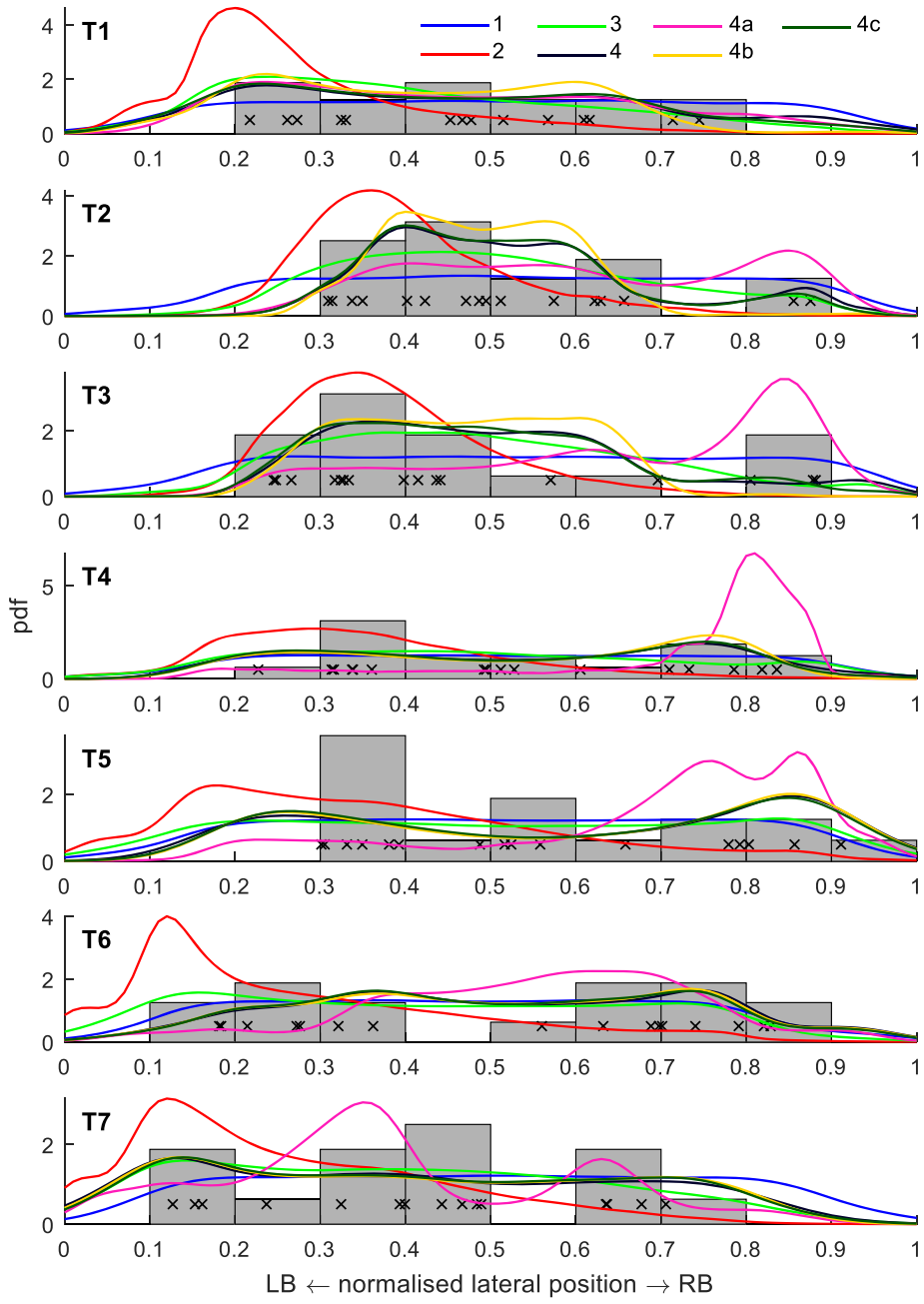

Fig. 7. Probability density functions (pdf) of lamprey normalised lateral position (grey bars; black crosses indicate exact locations) as they transited upstream through each perpendicular transect (T1–7 – see Fig. 4) and approached a Crump weir and hydropower station. Coloured lines are the normalised lateral distributions predicted by each model (Model 1–4c). LB and RB are Left and Right Bank, respectively.

base model alone (Fig. 8b; Table 3). However, there was little difference in PIT deviation scores between Model 4b, 4c and Model 4 (Table 3). All the models erroneously predicted some detections at PIT antennas on the weir face, as no parameterisation lamprey were detected there (Fig. 8b).

When considering lateral, temporal and PIT deviation collectively, Model 4 was the best base model at predicting movement patterns of the parameterisation lamprey (Table 3). The addition of avoidance behaviours in Model 4a and Model 4b resulted in poorer predictive power than the base model alone (Table 3). Model 4c, which also included avoidance of shallow slow flow regions, was the best model overall (Table 3). However, the relative improvement in overall performance between Model 4 and 4c was small (normalised score: 0.96 and 1.00, respectively) (Table 3).

The lateral, temporal, and PIT deviation scores and rankings for the validation (Table 4) and parameterisation lamprey (Table 3) were similar for each model, indicating that trends in model performance were valid even when using non-parameterisation data and that the best models (e.g. Model 4 and 4c) have 'within-site' predictive power.

Given the deviation scores and rankings for the parameterisation and validation lamprey, Model 4 and sub model 4c were selected as candidates for further assessment using all available data (31 lamprey tracks). Overall, both models performed considerably better than the null model (Model 1: uniform distribution) (Table 5). Model 4 was the best predictor of lamprey temporal and PIT distributions, with a much smaller mean error (2.7% and 6.6%, respectively) compared to Model 1 (10.2% and 18.8%, respectively) (Table 5). Model 4c was the best predictor of the lamprey lateral distribution, with a mean error of 4.4% compared to

Table 3
Lateral, temporal, PIT and mean deviation (normalised score [NS] and ranks) between the predicted (Model 1–4c) and observed distributions of parameterisation lamprey ($n = 16$) as they swam upstream and approached a Crump weir and hydropower station.

Model	Deviation scores Lateral (NS-rank)	Temporal (NS – rank)	PIT (NS - rank)	Mean (NS – rank)
1	0.0634 (0.00 – 5th)	0.1225 (0.00 – 7th)	0.1875 (0.00 – 5th)	0.1245 (0.00 – 7th)
2	0.0811 (−2.09 – 7th)	0.0379 (0.83 – 5th)	0.2445 (−5.00 – 7th)	0.1212 (0.05 – 6th)
3	0.0595 (0.49 – 4th)	0.0282 (0.92 – 2nd)	0.2140 (−0.23 – 6th)	0.1006 (0.32 – 5th)
4	0.0560 (0.92 – 2nd)	0.0291 (0.91 – 3rd)	0.0735 (1.00 – 1st)	0.0529 (0.96 – 2nd)
4a	0.0741 (−1.25 – 6th)	0.0852 (0.37 – 6th)	0.1000 (0.77 – 4th)	0.0865 (0.51 – 4th)
4b	0.0578 (0.70 – 3rd)	0.0308 (0.90 – 4th)	0.0775 (0.96 – 3rd)	0.0554 (0.93 – 3rd)
4c	0.0553 (1.00 – 1st)	0.0204 (1.00 – 1st)	0.0740 (0.99 – 2nd)	0.0499 (1.00 – 1st)

Table 4
Lateral, temporal, PIT and mean deviation (normalised scores [NS] and ranks) between the predicted (Model 1–4c) and observed distributions of validation lamprey ($n = 15$) as they swam upstream and approached a Crump weir and the hydropower station.

Model	Model deviation Lateral (NS - rank)	Temporal (NS - rank)	PIT (NS - rank)	Mean (NS - rank
1	0.0580 (0.00 – 5th)	0.0867 (0.00 – 7th)	0.1875 (0.00 – 5th)	0.1106 (0.00 – 6th)
2	0.0794 (−2.84 – 7th)	0.0692 (0.54 – 5th)	0.2444 (−0.48 – 7th)	0.1310 (−0.40 – 7th)
3	0.0528 (0.61 – 3rd)	0.0725 (0.44 – 6th)	0.2135 (−0.22 – 6th)	0.1129 (0.05 – 5th)
4	0.0504 (0.92 – 2nd)	0.0578 (0.90 – 3rd)	0.0713 (0.98 – 2nd)	0.0598 (0.98 – 2nd)
4a	0.0613 (−0.49 – 6th)	0.0635 (0.72 – 4th)	0.0695 (1.00 – 1st)	0.0648 (0.88 – 4th)
4b	0.0546 (0.37 – 4th)	0.0575 (0.91 – 2nd)	0.0717 (0.98 – 3rd)	0.0613 (0.96 – 3rd)
4c	0.0498 (1.00 – 1st)	0.0546 (1.00 – 1st)	0.0726 (0.97 – 4th)	0.0590 (1.00 – 1st)

5.0% for Model 1 (Table 5). Closer inspection of the lateral distributions at each perpendicular transect revealed that Model 4 and 4c produced similar results, and that at T1 and T4–7 there was little difference ($\pm <$ 1.2% mean error) between what they predicted and the null model (Fig. 9). However, for T2 and T3, where lamprey position was non-random (Fig. 4), both models more accurately reproduced their lateral distribution, reducing the mean spatial error from 6.1% to ca. 2.0% and 6.2% to ca. 4.0%, respectively (Fig. 9). The small additional reduction in lateral error produced by Model 4c compared to 4 can likely be attributed to some additional avoidance of regions near the true right bank in T1–4 (Fig. 9). When considering lateral, temporal and PIT deviation collectively using all lamprey data, Model 4, the simpler model, was the best model overall (Table 5).

4. Discussion

This study used POM to investigate the space use and behavioural response of upstream migrating European river lamprey to the hydrodynamic conditions encountered downstream of an instream barrier. Three emergent patterns were used to test model performance: 1) lateral distribution across the channel width, 2) passage time through a hydrophone array, and 3) location of first PIT detection at the instream structure. Lamprey tended to be relatively evenly distributed laterally across the channel as they migrated upstream and approached the obstruction, exhibiting a non-random distribution at only two out of seven locations. At these locations, lamprey were less frequently detected in the recirculating low-flow-velocity regions that occurred near the banks. Median passage time through the system was *ca.* 6

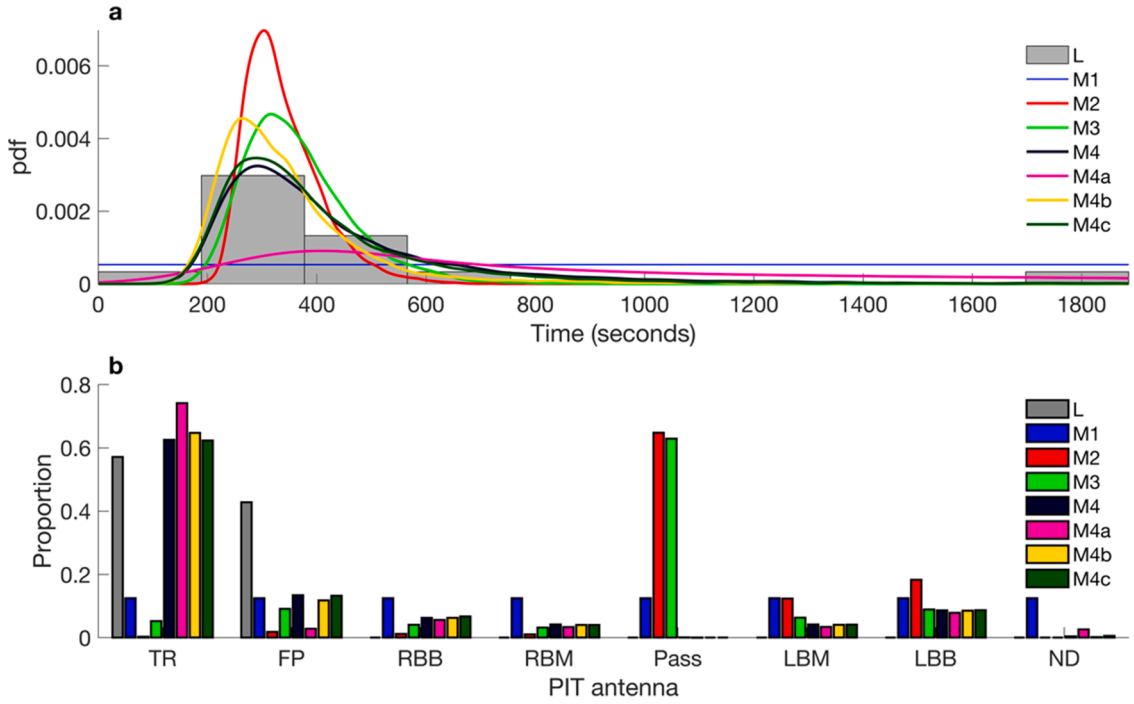

Fig. 8. a) Probability density function (pdf) of passage time for lamprey (L: grey bars) between transects T1 and T7, calculated from the processed acoustic telemetry tracks, as they transited upstream and approached a Crump weir and hydropower station. Coloured lines are temporal distributions predicted by each model (Model 1–4c). b) Distribution of first PIT detections at the weir, fish pass and hydropower station for lamprey (L: grey bars) and for each Model (coloured bars). TR: Tailrace; FP: Fish Pass; RBB: Right bank bankside, RBM: Right bank mid-channel; Pass: passed upstream over the weir; LBM: Left bank mid-channel; LBB: Left bank bankside; ND: Not detected.

Table 5
Mean error (percent) between predicted and observed lateral, temporal and PIT distributions (plus mean overall error), for Models 1 (null model: uniform distribution) and 4 and 4c (the best performing base model and sub model). NS and R are the normalised error score and rank, respectively, for each distribution.

Model	Lateral distribution			Temporal distribution			PIT distribution			Overall		
	Mean error (%)	NS	R	Mean error (%)	NS	R	Mean error (%)	NS	R	Mean error (%)	NS	R
1	4.95	0.00	3rd	10.19	0.00	3rd	18.75	0.00	3rd	11.3	0.00	3rd
4	4.53	0.73	2nd	2.65	1.00	1st	6.57	1.00	1st	4.58	1.00	1st
4c	4.37	1.00	1st	2.79	0.98	2nd	6.67	0.99	2nd	4.61	0.99	2nd

minutes and first PIT detections mostly occurred at the downstream end of the fish pass (50%) or in the hydropower tailrace (47%). The best performing model that reproduced the observed patterns (Model 4) was a spatially explicit Eulerian-Lagrangian Individual Based Model (IBM) that included two simple behaviours: 1) tortuous non-directed swimming when in low flow velocity (< 0.1 m s^{-1}) and 2) persistent directed (against the flow) swimming in moderate to high flow velocity (> 0.1 m s^{-1}).

The spatial distribution of European river lamprey as they moved upstream was similar to that reported for other lamprey species (*Petromyzon marinus*: Holbrook et al., 2015) but notably different to that of other families. For example, salmonids (*Oncorhynchus tshawytscha* and *Oncorhynchus nerka*: (Hughes, 2004), juvenile anguillids (*Anguilla anguilla*: Piper et al., 2012), and acipenserids (*Scaphirhynchus albus*: McElroy et al., 2012) tend to migrate upstream close to the channel edges, most likely to reduce energy expenditure by taking advantage of the low flow velocities that occur near the bank. Lamprey exhibited a relatively even across channel distribution as they moved upstream and did not obviously utilise near bank low flow regions. Indeed, they infrequently moved through near-bank low-flow-velocity recirculation regions, despite these areas potentially offering an energy efficient migration route. It is currently unclear if they are actively avoiding such regions or preferentially choosing other routes (e.g. selecting for higher velocities). Lamprey typically migrate upstream in unobstructed rivers near the bed boundary (Holbrook et al., 2015) where velocities are low, and therefore it is possible that they do not need to take advantage of near-bank low-velocity routes. However, acipenserids are also typically bed oriented during their upstream migration (McElroy et al., 2012) and juvenile eel are known to use bed-boundary conditions as they move upstream (Harrison et al., 2014; Vezza et al., 2020). It is likely that additional factors, not just energetics, are influencing lamprey movement in these areas. One potential reason why lamprey avoid recirculating low-velocity-regions is that they may become disoriented if local flow direction is unrepresentative of the bulk flow direction, which could result in delayed migration. This is exemplified by downstream moving juvenile salmonids that display more tortuous swimming and increased migration delay when flow velocities are very low in dam reservoirs (Ben Jebria et al., 2021). Further work is required to understand the evolutionary advantages of lamprey movement patterns, which differ from other upstream migrating species.

The median delay between last acoustic and first PIT detection (10.7 min) was greater than passage time through the array (5.8 min), indicating more complex movement trajectories occurred near the weir. Complex movement behaviour near obstructions is commonly exhibited by other aquatic species. For example, downstream moving European eel switch from exhibiting semi-passive movements as they approach a barrier to an exploratory 'search' behaviour and avoidance on encountering abrupt velocity gradients (Piper et al., 2015). Sea lamprey also switch from consistent steady swimming in slow flow to alternating between short burst movements and periods of rest when flow velocities are rapid near obstructions (Quintella et al., 2009; Kemp et al., 2011). High-resolution spatial-temporal tracking (< 1 m precision; *ca.* 1 Hz) directly downstream of the weir would have enabled quantification of alternative near-barrier behaviours but this was not possible using the equipment available due to the high levels of air entrainment in this region. In addition to likely exhibiting complex near-barrier behaviours, after their initial upstream movement and prior to PIT detection almost half of the lamprey were detected moving back downstream through the hydrophone array, with multiple movements up and downstream over several days being relatively common. This suggests that large scale 'searching' for passage routes is also part of the behavioural repertoire of European river lamprey when they encounter a barrier, as suggested for sea lamprey (Davies et al., 2021).

The hydrodynamic environment at the study site was complex, caused by a meandering channel, variable water depth and spatially uneven discharge from the weir and hydropower station. Fluctuating discharge throughout the study period also caused considerable temporal variability in water depth, channel width and hydrodynamics encountered by each lamprey. The range of discharges that occurred during the study period (10.4 to 52.3 m^3 s^{-1}) was not uncommon for the time of year at this site with both lower (*ca.* 3 m^3 s^{-1}: Lothian et al., 2020) and higher (*ca.* 60 m^3 s^{-1}: Tummers et al., 2016b) discharges recorded during similar periods in other years. During the study period, the highest predicted depth averaged velocity in the vicinity of the hydrophone array was similar under all discharges (*ca.* 1.15 m s^{-1}) and was focussed mid-channel or on the inside of the first bend downstream of the weir. Open channel flume experiments have found that river lamprey can progress upstream against flow velocities that range between 1.75 and 2.12 m s^{-1} (Russon and Kemp, 2011) with flows of 2.43 m s^{-1} blocking their movement (Kerr et al., 2015). Hence, it is likely that flow velocity wasn't a significant barrier to their movement in the vicinity of the hydrophone array. Within the tail race and fish pass and on the downstream weir face, predicted maximum depth averaged velocity ranged from 0.1−0.4 m s^{-1}, 2.0–2.9 m s^{-1}, and 4.3–5.6 m s^{-1}, respectively, between flow scenarios. The high predicted velocity at the fish pass and weir in comparison to lamprey swimming ability, supports previous evidence of very low passage efficiency via these routes at this site (unmodified fish pass: 0.3–1.5%: Tummers et al., 2016b; 2018; unmodified weir: 8.6%: Tummers et al., 2018).

Model 4 best predicted the upstream movement patterns of lamprey as they approached the weir. This spatially explicit Eulerian-Lagrangian IBM accommodated two simple swimming behaviours: 1) tortuous non-directed swimming when in low flow velocity and 2) persistent directed (against the flow) swimming in moderate to high flow velocity. The key spatial distribution patterns observed that were reproduced using these simple rules was a relatively even across channel distribution combined with the avoidance of near-bank low-flow-velocity recirculating regions. The idea that simple rules at the individual-level can produce complex emergent patterns is a crucial part of complexity theory, the study of complex systems (Herbert-Read, 2016). In the field of aquatic movement ecology, there has been a tendency to statistically identify and propose an overly complex array of hydrodynamic metrics that could influence space use (see Kerr et al., 2016). The results of this study, in line with the principles of complexity theory, highlight that basic rules are often sufficient to reproduce emergent patterns. Additional movement rules, such as the avoidance of shallow slow flow regions (Model 4c), slightly improved spatial distribution predictions but not overall model performance. Model assessment and validation were carried out using a random subset of the fish movement data. This constrains validation to the specific field site and range of hydrodynamic conditions that occurred during the study. It is recommended that further validation of Model 4 occurs using data acquired at other sites. It is also worth noting

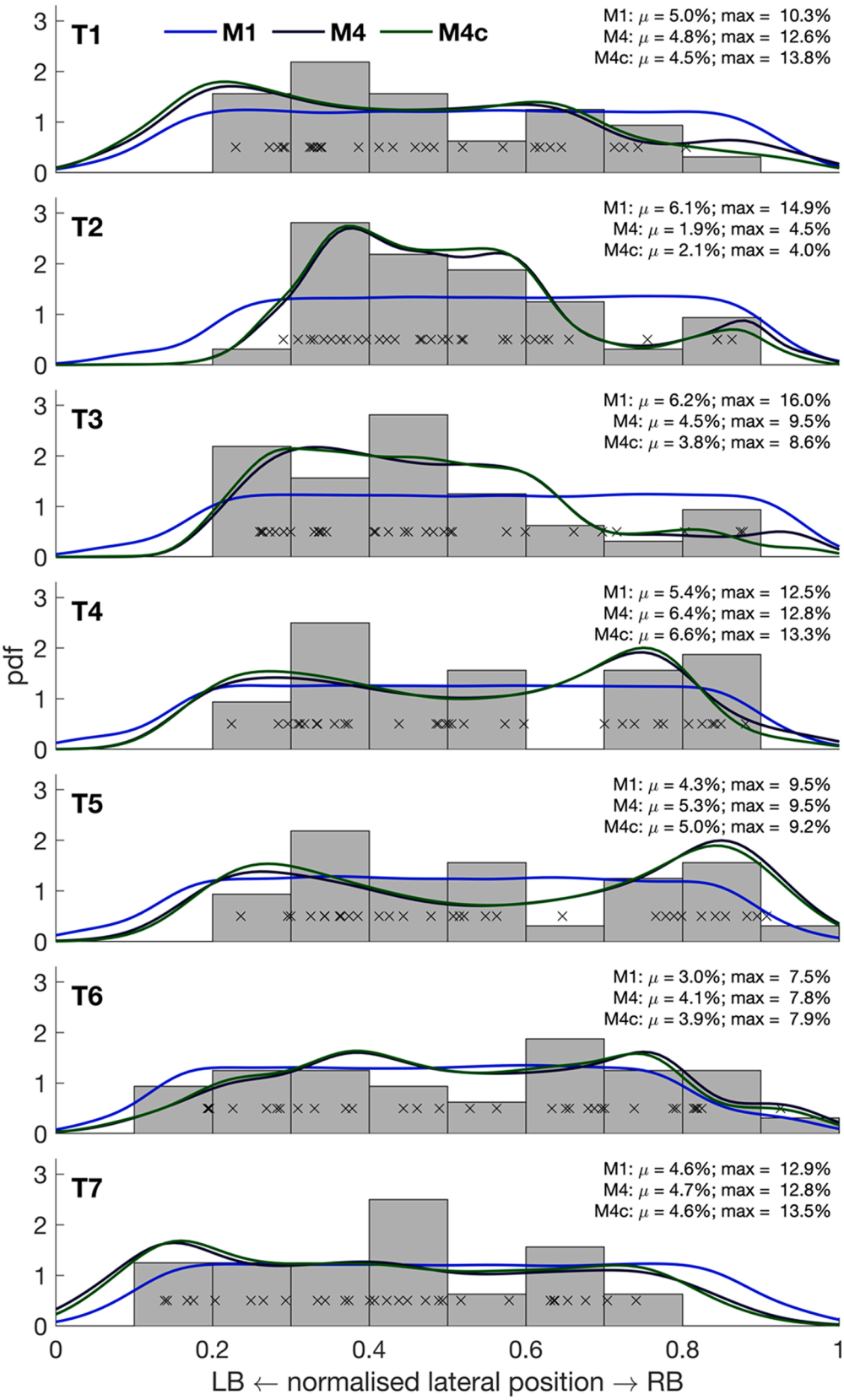

Fig. 9. Probability density functions (pdf) of normalised lateral position (grey bars; black crosses indicate exact locations) for all lamprey ($n = 31$) as they moved upstream through perpendicular transects (T1–7 – see Fig. 4) and approached a Crump weir and hydropower station. Coloured lines are the normalised lateral distributions predicted by Model 1 (blue), 4 (black) and 4c (green). LB and RB are Left and Right Bank, respectively. Inset text is the mean (μ) and maximum (max) error between the observed and modelled distributions for each transect for Model 1, 4 and 4c.

that Model 4 will only be applicable for predicting lamprey movements when they are actively migrating upstream during their spawning migration. For other lifestages and movements (e.g. for downstream moving transformers, downstream 'searching' behaviour, or prey seeking at sea), Model 4 would be inappropriate as a lamprey's motivation and response to hydrodynamics is likely vastly different in these situations.

Hydrodynamics are frequently a key predictor of space use by fish (e.g. McElroy et al., 2012; Goodwin et al., 2014; Silva et al., 2020) but it was uncertain to what extent this would be the case for lamprey, as they are thigmotactic and can move upstream by attaching to hard surfaces using their oral disk, and resting between intermittent bouts of activity (Quintella et al., 2009; Kerr et al., 2015). The results of this study highlight that hydrodynamics are a crucial predictor of lamprey space use, as the flow dependant base model (Model 4) performed well, whereas those where agents moved independent of flow (i.e. using ground speed and direction distributions) (e.g. Models 2 and 3) did not. This result is important as identifying what data are needed to guide conservation efforts is critical not only in implementing effective mitigation but also for resource allocation and decision making (e.g. Flanagan et al., 2018). The results of this study require validation at additional sites under a wider range of environmental conditions, but current evidence suggests that, when appropriate movement rules are used, depth averaged flow velocity and direction (i.e. available from a 2-D hydrodynamic model) are sufficient to predict the key movement patterns of European river lamprey as they migrate upstream.

Existing and widely used methods for predicting space use by lotic fish have typically been based on relatively simplistic statistical relationship between fish abundance and key environmental variables and they have been heavily criticised for this (e.g. PHABSIM: Railsback, 2016; Kemp and Katopodis, 2017; but also see Dray et al., 2010; Kerr et al., 2016). One flaw of these simplistic methods is the assumption that 'preference' for different environmental variables (e.g. depth, flow velocity, overhead cover) is independent (Mathur et al., 1985). For example, the PHABSIM methodology assumes that fish preference for certain depths is completely independent of the flow velocity at that location, yet empirical evidence indicates this is flawed (Capra et al., 2017). This study also provides direct evidence of the inaccuracy of this assumption. For example, a tentative assessment of the preference curves suggested that lamprey avoided both shallow and slow flow regions. However, two movement models (Model 4a and 4b) where rules were implemented to cause agents to avoid such conditions independently, performed poorly. It was only when these environmental variables were treated in combination, i.e. a rule was implemented where agents avoided areas where both depth and flow velocity were low (Model 4c), that any improvement in model performance was observed. The improvement in model performance was marginal (isolated to lamprey lateral distribution) but the results provide evidence for the inaccuracy of the assumption of independence of environmental variables. They also highlight the importance of systematically testing movement hypotheses, something that is required as part of the POM process and easily achieved using spatially explicit IBMs.

Mitigation measures to offset the impacts of aquatic habitat fragmentation are frequently ineffective (e.g. Brown et al., 2013; Lusardi and Moyle, 2017), often due to a poor understanding of fish behaviour in response to hydrodynamics, resulting in a lack of transferability of technology (Kemp, 2016b). The methods used in this study, a combination of field telemetry, hydrodynamic modelling, and POM, enabled systematic identification of the key hydrodynamic and behavioural factors that governed the space use of the target species. The results represent a substantial step forward in our knowledge on how the target species move as they approach an instream barrier and will aid in the development of more effective mitigation. The methods used were effective and represent a useful framework for investigating similar relationships in other aquatic species.

CRediT authorship contribution statement

J.R. Kerr: Conceptualization, Methodology, Software, Formal analysis, Investigation, Writing – original draft, Writing – review & editing, Visualization, Project administration. **J.S. Tummers:** Methodology, Investigation, Writing – original draft, Writing – review & editing. **T. Benson:** Methodology, Software, Formal analysis, Investigation, Writing – original draft, Writing – review & editing, Visualization. **M.C. Lucas:** Conceptualization, Methodology, Investigation, Resources, Writing – original draft, Writing – review & editing, Supervision, Project administration, Funding acquisition. **P.S. Kemp:** Conceptualization, Methodology, Resources, Writing – original draft, Writing – review & editing, Supervision, Project administration, Funding acquisition.

Declaration of Competing Interest

The authors declare that they have no known competing financial interests or personal relationships that could have appeared to influence the work reported in this paper.

Data availability

Supporting data for this study are openly available from the University of Southampton repository at https://doi.org/10.5258/SOTON/D2449.

Acknowledgements

This research was primarily funded by the Horizon 2020 AMBER (Adaptive Management of Barriers in European Rivers) project (no. 689682). Additional funding for equipment and researcher time was provided by the Environment Agency, University of Durham, and HR Wallingford. We are grateful to George Winn-Darley and Greg McCormick for site access, Jon Hateley (Environment Agency) for the loan of extra telemetry equipment, Pat O'Brien (Environment Agency) for project support, and Chris Train (Environment Agency) for allowing us to use the hydrometry building to house our equipment. We are also hugely grateful to members of the International Centre for Ecohydraulics Research (University of Southampton) and University of Durham for assistance with field work.

Supplementary materials

Supplementary material associated with this article can be found, in the online version, at doi:10.1016/j.ecolmodel.2022.110210.

References

Belletti, B., Garcia de Leaniz, C., Jones, J., et al., 2020. More than one million barriers fragment Europe's rivers. Nature 588, 436–441. https://doi.org/10.1038/s41586-020-3005-2.

Ben Jebria, N., Carmigniani, R., Drouineau, H., De Oliveira, E., Tétard, S., Capra, H., 2021. Coupling 3D hydraulic simulation and fish telemetry data to characterize the behaviour of migrating smolts approaching a bypass. J. Ecohydraulics, 1978345. https://doi.org/10.1080/24705357.2021.1978345.

Benson, T., de Bie, J., Gaskell, J., et al., 2021. Agent-based modelling of juvenile eel migration via selective tidal stream transport. Ecol. Modell. 443, 109448 https://doi.org/10.1016/j.ecolmodel.2021.109448.

Beyer, H.L., Haydon, D.T., Morales, J.M., Frair, J.L., Hebblewhite, M., Mitchell, M., Matthiopoulos, J., 2010. The interpretation of habitat preference metrics under use–availability designs. Philos. Trans. R. Soc. Lond. A 365, 2245–2254. https://doi.org/10.1098/rstb.2010.0083.

Boubeè, J., Jellyman, D., Sinclair, C., 2008. Eel protection measures within the Manapouri hydro-electric power scheme, South Island, New Zealand. Hydrobiologia 609, 71–82. https://doi.org/10.1007/s10750-008-9400-6.

Bracken, F.S.A., Hoelzel, A.R., Hume, J.B., Lucas, M.C., 2015. Contrasting population genetic structure among freshwater-resident and anadromous lampreys: the role of demographic history, differential dispersal, and anthropogenic barriers to movement. Mol. Ecol. 24, 1188–1204. https://doi.org/10.1111/mec.13112.

Brosnan, I.G., Welch, D.W., 2020. A model to illustrate the potential pairing of animal biotelemetry with individual-based modeling. Anim. Biotelemetry 8, 36. https://doi.org/10.1186/s40317-020-00221-z.
Brown, J.J., Limburg, K.E., Waldman, J.R., Stephenson, K., Glenn, E.P., Juanes, F., Jordaan, A., 2013. Fish and hydropower on the U.S. Atlantic coast: failed fisheries policies from half-way technologies. Conserv. Lett. 6 (4), 280–286. https://doi.org/10.1111/conl.12000.
Capra, H., Plichard, P., Bergé, J., Pella, H., Ovidio, M., McNeil, E., Lamouroux, N., 2017. Fish habitat selection in a large hydropeaking river: strong individual and temporal variations revealed by telemetry. Sci. Total Environ. 578, 109–120. https://doi.org/10.1016/j.scitotenv.2016.10.155.
Codling, E.A., Plank, M.J., Benhamou, S., 2008. Random walk models in biology. J. R. Soc., Interface 5, 813–834. https://doi.org/10.1098/rsif.2008.0014.
Davies, P., Britton, J.R., Nunn, A.D., et al., 2021. Cumulative impacts of habitat fragmentation and the environmental factors affecting upstream migration in the threatened sea lamprey, *Petromyzon marinus*. Aquat. Conserv. 31, 2560–2574. https://doi.org/10.1002/aqc.3625.
DeAngelis, D.L., Yurek, S., 2017. Spatially Explicit Modeling in Ecology: a Review. Ecosystems 20, 284–300. https://doi.org/10.1007/s10021-016-0066-z.
Deinet, S., Scott-Gatty, K., Rotton, H., et al., 2020. The Living Planet Index (LPI) For Migratory Freshwater Fish - Technical Report. World Fish Migration Foundation, The Netherlands, p. 55.
Dray, S., Royer-Carenzi, M., Calenge, C., 2010. The exploratory analysis of autocorrelation in animal-movement studies. Ecol. Res. 25, 673–681. https://doi.org/10.1007/s11284-010-0701-7.
Dye, B., Jose, F., Richard, J., Mortensen, J.B., Milbrandt, E.C., 2022. An agent-based model accurately predicts larval dispersal and identifies restoration and monitoring priorities for eastern oyster (*Crassostrea virginica*) in a Southwest Florida estuary. Restor. Ecol. 30, e13487. https://doi.org/10.1111/rec.13487.
Finger, J.S., Dhellemmes, F., Guttridge, T.L., Kurvers, R.H.J.M., Gruber, S.H., Krause, J., 2016. Rate of movement of juvenile lemon sharks in a novel open field, are we measuring activity or reaction to novelty? Anim. Behav. 116, 75–82. https://doi.org/10.1016/j.anbehav.2016.03.032.
Flanagan, S.P., Forester, B.R., Latch, E.K., Aitken, S.N., Hoban, S., 2018. Guidelines for planning genomic assessment and monitoring of locally adaptive variation to inform species conservation. Evol. Appl. 11, 1035–1052. https://doi.org/10.1111/eva.12569.
Fluker, B.L., Kuhajda, B.R., Harris, P.M., 2014. The effects of riverine impoundment on genetic structure and gene flow in two stream fishes in the Mobile River basin. Freshwater Biol. 59, 526–543. https://doi.org/10.1111/fwb.12283.
Gao, Z., Andersson, H.I., Dai, H., Jiang, F., Zhao, L., 2016. A new Eulerian–Lagrangian agent method to model fish paths in a vertical slot fishway. Ecol. Eng. 88, 217–225. https://doi.org/10.1016/j.ecoleng.2015.12.038.
Goodwin, R.A., Politano, M., Garvin, J.W., et al., 2014. Fish navigation of large dams emerges from their modulation of flow field experience. Proc. Natl. Acad. Sci. U.S.A. 111, 5277–5282. https://doi.org/10.1073/pnas.1311874111.
Goerig, E., Castro-Santos, T., 2017. Is motivation important to brook trout passage through culverts? Can. J. Fish. Aquat.Sci. 74 (6), 885–893. https://doi.org/10.1139/cjfas-2016-0237.
Grill, G., Lehner, B., Thieme, M., et al., 2019. Mapping the world's free-flowing rivers. Nature 569, 215–221. https://doi.org/10.1038/s41586-019-1111-9.
Grimm, V., Railsback, S.F., 2012. Pattern-oriented modelling: a 'multi-scope' for predictive systems ecology. Philos. Trans. R. Soc. B 367, 298–310. https://doi.org/10.1098/rstb.2011.0180.
Gurarie, E., Andrews, R.D., Laidre, K.L., 2009. A novel method for identifying behavioural changes in animal movement data. Ecol. Lett. 12, 395–408. https://doi.org/10.1111/j.1461-0248.2009.01293.x.
Gustafson, R.G., Waples, R.S., Myers, J.M., Weitkamp, L.A., Bryant, G.J., Johnson, O.W., Hard, J.J., 2007. Pacific salmon extinctions: quantifying lost and remaining diversity. Conserv. Biol. 21 (4), 1009–1020. https://doi.org/10.1111/j.1523-1739.2007.00693.x.
Harrison, A.J., Walker, A.M., Pinder, A.C., Briand, C., Aprahamian, M.W., 2014. A review of glass eel migratory behaviour, sampling techniques and abundance estimates in estuaries: implications for assessing recruitment, local production and exploitation. Rev. Fish Biol. Fish. 24 https://doi.org/10.1007/s11160-014-9356-8.
Herbert-Read, J.E., 2016. Understanding how animal groups achieve coordinated movement. J. Exp. Biol. 219, 2971–2983. https://doi.org/10.1242/jeb.129411.
Holbrook, C.M., Bergstedt, R., Adams, N.S., Hatton, T.W., McLaughlin, R.L., 2015. Fine-scale pathways used by adult sea lampreys during riverine spawning migrations. Trans. Am. Fish Soc. 144, 549–562. https://doi.org/10.1080/00028487.2015.1017657.
Hughes, N.F., 2004. The wave-drag hypothesis: an explanation for size-based lateral segregation during the upstream migration of salmonids. Can. J. Fisheries Aquat. Sci. 61, 103–109. https://doi.org/10.1139/f03-144.
Jellyman, D.J., Ryan, C.M., 1983. Seasonal migration of elvers (*Anguilla* spp.) into Lake Pounui, New Zealand, 1974-1978. N. Z. J. Mar. Freshwater Res. 17 (1), 1–15. https://doi.org/10.1080/00288330.1983.9515981.
Katz, J., Moyle, P.B., Quiñous, R.M., Israel, J., Purdy, S., 2013. Impending extinction of salmon, steelhead, and trout (Salmonidae) in California. Environ. Biol. Fishes 96, 1169–1186. https://doi.org/10.1007/s10641-012-9974-8.
Keefer, M.L., Peery, C.A., Lee, S.R., Daigle, W.R., Johnson, E.L., Moser, M.L., 2011. Behaviour of adult Pacific lamprey in near-field flow and fishway design experiments. Fish. Manag. Ecol. 18, 177–189. https://doi.org/10.1111/j.1365-2400.2010.00772.x.
Kemp, P.S., Tsuzaki, T., Moser, M.L., 2009. Linking behaviour and performance: intermittent locomotion in a climbing fish. J. Zool. 277, 171–178. https://doi.org/10.1111/j.1469-7998.2008.00525.x.
Kemp, P.S., Russon, I.J., Vowles, A.S., Lucas, M.C., 2011. The influence of discharge and temperature on the ability of upstream migrant adult river lamprey (*Lampetra fluviatilis*) to pass experimental overshot and undershot weirs. River Res. Appl. 27, 488–498. https://doi.org/10.1002/rra.1364.
Kemp, P.S., 2012. Bridging the gap between fish behaviour, performance and hydrodynamics: an ecohydraulics approach to fish passage research. River Res. Appl. 28 (4), 403–406. https://doi.org/10.1002/rra.1599.
Kemp, P.S. 2016a. Impoundments, barriers and abstractions: impact on fishes and fisheries, mitigation and future directions. Chapter 7.5. In: Freshwater Fisheries Ecology, 1st Edition. Ed.: Craig, J.F. 717–769. https://doi.org/10.1002/9781118394380.ch52.
Kemp, P.S., 2016b. Meta-analyses, metrics and motivation: mixed messages in the fish passage debate. River Res. Appl. 32, 2116–2124. https://doi.org/10.1002/rra.3082.
Kemp, P.S., Katopodis, C., 2017. Environmental flows all at sea? Charting a new course through choppy waters. J. Ecohydraulics 2 (2), 85–87. https://doi.org/10.1080/24705357.2017.1383684.
Kerr, J.R., Karageorgopoulos, P., Kemp, P.S., 2015. Efficacy of a side-mounted vertically oriented bristle pass for improving upstream passage of European eel (*Anguilla anguilla*) and river lamprey (*Lampetra fluviatilis*) at an experimental crump weir. Ecol. Eng. 85, 121–131. https://doi.org/10.1016/j.ecoleng.2015.09.013.
Kerr, J.R., Manes, C., Kemp, P.S., 2016. Assessing hydrodynamic space use of brown trout, Salmo trutta, in a complex flow environment: a return to first principles. J. Exp. Biol. 219, 3480–3491. https://doi.org/10.1242/jeb.134775.
Kerr, J.R., Vowles, A.S., Crabb, M.C., Kemp, P.S., 2021. Selective fish passage: restoring habitat connectivity without facilitating the spread of a non-native species. Environ. Manage. 279, 110908 https://doi.org/10.1016/j.jenvman.2020.110908.
Klopries, E.-M., Deng, Z.D., Lachmann, T.U., Schüttrumpf, H., Trumbo, B.A., 2018. Surface bypass as a means of protecting downstream migrating fish: lack of standardised evaluation criteria complicates evaluation of efficacy. Mar. Freshwater Res. 69, 1882–1893. https://doi.org/10.1071/mf18097.
Langdon, S.A., Collins, A.L., 2000. Quantification of the maximal swimming performance of Australasian glass eels, *Anguilla australis* and *Anguilla reinhardtii*, using a hydraulic flume swimming chamber. N. Z. J. Mar. Freshwater Res. 34 (4), 629–636. https://doi.org/10.1080/00288330.2000.9516963.
Liermann, C.R., Nilsson, N., Robertson, J., Ng, R.Y., 2012. Implications of Dam Obstruction for Global Freshwater Fish Diversity. Bioscience 62 (6), 539–548. https://doi.org/10.1525/bio.2012.62.6.5.
Lothian, A.J., Tummers, J.S., Albright, A.J., O'Brien, P., Lucas, M.C., 2020. River connectivity restoration for upstream-migrating European river lamprey: the efficacy of two horizontally-mounted studded tile designs. River Res. Appl. 36, 2013–2023. https://doi.org/10.1002/rra.3734.
Lucas, M.C., Bubb, D.H., Jang, M., Ha, K., Masters, J.E.G., 2009. Availability of and access to critical habitats in regulated rivers: effects of low-head barriers on threatened lampreys. Freshwater Biol. 54, 621–634. https://doi.org/10.1111/j.1365-2427.2008.02136.x.
Lusardi, R.A., Moyle, P.B., 2017. Two-way trap and haul as a conservation strategy for anadromous salmonids. Fisheries 2 (9), 478–487. https://doi.org/10.1080/03632415.2017.1356124.
Manly, B.F., 2007. Randomization, Bootstrap and Monte Carlo Methods in Biology. CRC Press, Boca Raton, Florida. https://doi.org/10.1201/9781315273075.
Masters, J.E.G., Jang, M.-.H., Ha, K., Bird, P.D., Frear, P.A., Lucas, M.C., 2006. The commercial exploitation of a protected anadromous species, the river lamprey (*Lampetra fluviatilis* (L.)), in the tidal River Ouse, North East England. Aquat. Conserv. 16, 77–92. https://doi.org/10.1002/aqc.686.
Mathur, D., Bason, W.H., Purdy Jr., E.J., Silver, C.A, 1985. A critique of the Instream Flow Incremental Methodology. Can. J. Fisheries Aquat. Sci. 42, 825–831. https://doi.org/10.1139/f85-105.
McElroy, B., DeLonay, A., Jacobson, R., 2012. Optimum swimming pathways of fish spawning migrations in rivers. Ecology 93 (1), 29–34. https://doi.org/10.1890/11-1082.1.
Morrice, K.J., Baptista, A.M., Burke, B.J., 2020. Environmental and behavioral controls on juvenile Chinook salmon migration pathways in the Columbia River estuary. Ecol. Modell. 427, 109003 https://doi.org/10.1016/j.ecolmodel.2020.109003.
Muir, W.D., Smith, S.G., Williams, J.G., Sandford, B.P., 2001. Survival of juvenile salmonids passing through bypass systems, turbines, and spillways with and without flow deflectors at Snake River dams. North Am. J. Fisheries Manag. 21 (1), 135–146. https://doi.org/10.1577/1548-8675(2001)021<0135:sojspt>2.0.co;2.
Noonan, M.J., Grant, J.W.A., Jackson, C.D., 2012. A quantitative assessment of fish passage efficiency. Fish Fisheries 13, 450–464. https://doi.org/10.1111/j.1467-2979.2011.00445.x.
Padgett, T.E., Thomas, R.E., Borman, D.J., Mould, D.C., 2020. Individual-based model of juvenile eel movement parameterized with computational fluid dynamics-derived flow fields informs improved fish pass design. R. Soc. Open Sci. 7, 191505 https://doi.org/10.1098/rsos.191505.
Pereira, E., Quintella, B.R., Mateus, C.S., Alexandre, C.M., Belo, A.F., Telhado, A., Quadrado, M.F., Almeida, P.R., 2017. Performance of a vertical-slot fish pass for the sea lamprey *Petromyzon marinus* L. and habitat recolonization. River Res. Appl. 33, 16–26. https://doi.org/10.1002/rra.3054.

Piper, A.T., Wright, R.M., Kemp, P.S., 2012. The influence of attraction flow on upstream passage of European eel (*Anguilla anguilla*) at intertidal barriers. Ecol. Eng. 44, 329–336. https://doi.org/10.1016/j.ecoleng.2012.04.019.

Piper, A.T., Manes, C., Siniscalchi, F., Marion, A., Wright, R.M., Kemp, P.S., 2015. Response of seaward-migrating European eel (*Anguilla anguilla*) to manipulated flow fields. Proc. R. Soc. B 282, 20151098. https://doi.org/10.1098/rspb.2015.1098.

Quintella, B.R., Póvoa, I., Almeida, P.R., 2009. Swimming behaviour of upriver migrating sea lamprey assessed by electromyogram telemetry. J. Appl. Ichthyol. 25, 46–54. https://doi.org/10.1111/j.1439-0426.2008.01200.x.

Raderschall, C.A., Magrath, R.D., Hemmi, J.M., 2011. Habituation under natural conditions: model predators are distinguished by approach direction. J. Exp. Biol. 214 (24), 4209–4216. https://doi.org/10.1242/jeb.061614.

Railsback, S., 2016. Why it is time to put PHABSIM out to pasture. Fisheries 41 (12), 720–725. https://doi.org/10.1080/03632415.2016.1245991.

Riotte-Lambert, L., Matthiopoulos, J., 2020. Environmental predictability as a cause and consequence of animal movement. Trends Ecol. Evol. 35 (2), 163–174. https://doi.org/10.1016/j.tree.2019.09.009.

Russon, I.J., Kemp, P.S., 2011. Experimental quantification of the swimming performance and behaviour of spawning run river lamprey *Lampetra fluviatilis* and European eel *Anguilla anguilla*. J. Fish Biol. 78, 1965–1975. https://doi.org/10.1111/j.1095-8649.2011.02965.x.

Sánchez-Bayoa, F., Wyckhuys, K.A.G., 2019. Worldwide decline of the entomofauna: a review of its drivers. Biol. Conserv. 232, 8–27. https://doi.org/10.1016/j.biocon.2019.01.020.

Ø. Silva, A.T., Bærum, K.M., Hedger, R.D., Baktoft, H., Fjeldstad, H.-P., Gjelland, K., Finn, Ø., Torbjør, F, 2020. The effects of hydrodynamics on the three-dimensional downstream migratory movement of Atlantic salmon Sci. Total Environ. 705, 135773 https://doi.org/10.1016/j.scitotenv.2019.135773.

Snyder, M.N., Schumaker, N.H., Ebersole, J.L., et al., 2019. Individual based modelling of fish migration in a 2-D river system: model description and case study. Landsc. Ecol. 34, 737–754. https://doi.org/10.1007/s10980-019-00804-z.

Tan, J., Tao, L., Gao, Z., Dai, H., Shi, X., 2018. Modeling fish movement trajectories in relation to hydraulic response relationships in an experimental fishway. Water (Basel) 10 (11), 1511. https://doi.org/10.3390/w10111511.

Tummers, J.S., Hudson, S. and Lucas. M.C. 2016a. Evaluating the effectiveness of restoring longitudinal connectivity for stream fish communities: towards a more holistic approach Science of the Total Environment, 569–570, 850–860. https://doi.org/10.1016/j.scitotenv.2016.06.207.

Tummers, J.S., Winter, E., Silva, S., O'Brien, P., Jang, M.H., Lucas, M.C., 2016b. Evaluating the effectiveness of a Larinier super active baffle fish pass for European river lamprey *Lampetra fluviatilis* before and after modification with wall-mounted studded tiles. Ecol. Eng. 91, 183–194. https://doi.org/10.1016/j.ecoleng.2016.02.046.

Tummers, J.S., Kerr, J.R., O'Brien, P., Kemp, P.S., Lucas, M.C., 2018. Enhancing the upstream passage of river lamprey at a microhydropower installation using horizontally-mounted studded tiles. Ecol. Eng. 125, 87–97. https://doi.org/10.1016/j.ecoleng.2018.10.015.

Vezza, P., Libardoni, F., Manes, C., et al., 2020. Rethinking swimming performance tests for bottom-dwelling fish: the case of European glass eel (*Anguilla anguilla*). Sci. Rep. 10, 16416. https://doi.org/10.1038/s41598-020-72957-w.

Vowles, A.S., Don, A.M., Karageorgopoulous, P., Kemp, P.S., 2017. Passage of European eel and river lamprey at a model weir provisioned with studded tiles. J. Ecohydraulics 2, 88–98. https://doi.org/10.1080/24705357.2017.1310001.

Vowles, A.S., Karageorgopoulos, P., Kemp, P.S., 2018. Upstream movement of river lamprey through a culvert retrofitted with spoiler baffles under experimental conditions. J. Ecohydraulics 3 (2), 99–107. https://doi.org/10.1080/24705357.2018.1555777.

White, E.M., Knights, B., 1997. Dynamics of upstream migration of the European eel, *Anguilla anguilla* (L.), in the Rivers Severn and Avon, England, with special reference to the effects of man-made barriers. Fish. Manag. Ecol. 4, 311–324. https://doi.org/10.1046/j.1365-2400.1997.00050.x.

Whitfield, R.E., Kolenosky, D.P., 1978. Prototype Eel Ladder in the St. Lawrence River. Progr. Fish-Culturist 40 (4), 152–154. https://doi.org/10.1577/1548-8659(1978)40[152:pelits]2.0.co;2.

Wilkes, M.A., Webb, J.A., Pompeu, P.S., Silva, L.G.M., Vowles, A.S., Baker, C.F., Franklin, P., Link, O., Kemp, P.S., 2018. Not just a migration problem: metapopulations, habitat shifts, and gene flow are also important for fishway science and management. River Res. Appl. 35, 1688–1696. https://doi.org/10.1002/rra.3320.

Williams, J.G., Armstrong, G., Katopodis, C., Larinier, M., Travade, F., 2012. Thinking like a fish: a key ingredient for development of effective fish passage facilities at river obstructions. River Res. Appl. 28, 407–417. https://doi.org/10.1002/rra.1551.

Wilson, M.C., Chen, X.Y., Corlett, R.T., et al., 2016. Habitat fragmentation and biodiversity conservation: key findings and future challenges. Landsc. Ecol. 31, 219–227. https://doi.org/10.1007/s10980-015-0312-3.

Zhang, H., Jarić, I., Roberts, D.L., He, Y., Du, H., Wu, J., et al., 2020. Extinction of one of the world's largest freshwater fishes: lessons for conserving the endangered Yangtze fauna. Sci. Total Environ. 710, 136242 https://doi.org/10.1016/j.scitotenv.2019.136242.